Computer Simulation of the Linear and Nonlinear Optical Susceptibilities of *p*-Nitroaniline in Cyclohexane, 1,4-Dioxane, and Tetrahydrofuran in Quadrupolar Approximation. I. Molecular Polarizabilities and Hyperpolarizabilities

H. Reis,* A. Grzybowski,† and M. G. Papadopoulos

Institute of Organic and Pharmaceutical Chemistry, National Hellenic Research Foundation, Vasileos Constantinou 48, GR-11635 Athens, Greece

Received: May 31, 2005; In Final Form: September 7, 2005

This is the first part of a study of the local field effects on (non)linear optical susceptibilities of solutions of *para*-nitroaniline (pNA) in three different solvents, cyclohexane (CH), 1,4-dioxane (DI), and tetrahydrofuran (THF), using a discrete molecular representation of the condensed phase. To account for dipolar and quadrupolar effects, the latter of which are especially important for DI solution, all the electric properties necessary to compute the local fields and local field gradients in quadrupolar approximation as well as the dipolar hyperpolarizabilities for the four molecules are computed, including frequency dispersion and vibrational contributions to the dipolar properties. The convergence of the perturbation treatment for the pure vibrational (PV) contributions is examined by comparison of the values obtained at the lowest order with those of partially computed second order in mechanical and electrical anharmonicity. For pNA, for which previous computations of the hyperpolarizabilities have generally found poor agreement with experimental results, a thorough investigation of the effects of solvent-induced geometry changes, dynamic and static correlation, frequency dispersion, and classical thermal averaging over the torsional modes of the substituent groups and the inversion mode of the amino group on the dipolar properties is carried out. Computations using self-consistent continuum reaction field models show that the amino group is substantially less pyramidalized in polar solvents than in the gas phase. With all the effects taken into account, reasonable agreement with the experimental electric-field induced second harmonic generation (EFISH) result on pNA vapor of Kaatz, Donley, and Shelton (*J. Chem. Phys*. **1997**, *108*, 849) is obtained.

Introduction

The computation of nonlinear optical properties (NLO) of molecular systems by quantum mechanical methods is already at a highly sophisticated level, yielding results for simple systems which are believed to reach and even surpass experimental accuracy.[1] Methods for the computation of NLO properties of condensed phases are still considerably lagging behind in accuracy. Local field effects, which are generally predominant in molecular liquids, have been computed in the framework of continuum models (e.g., refs 2 and 3) or using discrete local field models, which have emerged in recent years[4−9] and should in principle be more accurate than continuum models because of explicit consideration of the molecular structure in the liquid. The latter methods have been applied almost exclusively to pure liquids and, with the exception of the work on liquid water by Gubskaya and Kusalik,[6,10] in dipolar approximation. However, many experimental NLO property determinations are conducted in dilute solutions, using non-dipolar, but multipolar, solvents such as 1,4-dioxane. To treat such systems in the framework of discrete local field (DLF) models, the limitations mentioned above have to be lifted. This is the first part of a two-part series in which we extend one of the dipolar DLF models applied previoulsy to pure liquids[7,8] to higher multipolar order and multicomponent liquids and report an application to solutions of *p*-nitroaniline, the "fruit-fly" of organic nonlinear optics,[11] in three solvents of different multipolar character, that is, cyclohexane, 1,4-dioxane, and tetrahydrofuran.

The molecular properties of the constituent molecules are needed as input in the DLF model and determine to a large extent the accuracy of the obtained linear and nonlinear susceptibilities. In particular, the hyperpolarizabilities of *p*-nitroaniline still constitute a challenge for computational chemistry. Large discrepancies between computed and experimental values in 1,4-dioxane solution have been stated in the past, for example, by Sim et al.[12] in their study of the hyperpolarizabilities of pNA at the second-order Møller−Plesset (MP2) level, and were tentatively attributed to solvation effects. However, multiconfigurational self-consistent field (MCSCF) computations on the isolated molecule[13] and on the solvated molecule using a self-consistent reaction field (SCRF) method[3] still essentially failed to reproduce the experimental dispersion. Later, Salek et al.[14] claimed that a comparison of the experimental gas-phase value of Kaatz et al.[15] and the values obtained by Teng and Garito[16] in 1,4-dioxane solution shows that solvent effects in 1,4-dioxane are taken into account nearly entirely by the usual Lorentz−Onsager local field factors. This would in fact not be unreasonable, if 1,4-dioxane were not only a non-dipolar solvent, as its relative permittivity suggests, but more generally an "unpolar" solvent. However, there is a considerable amount of experimental evidence[17−20] suggesting that 1,4-dioxane is a multipolar solvent which acts like a dipolar solvent with a relative permittivity $\epsilon_r = 6-7$.[18,20] In addition, the claim

* Corresponding author. e-mail: hreis@eie.gr.
† Present address: Institute of Physics, Silesian University, ul. Uniwersytecka 4, 40-007 Katowice, Poland.

10.1021/jp052875b CCC: $30.25
Published on Web 10/18/2005

of Salek et al. is also not in accord with the experimental hyper-Rayleigh scattering work of Kaatz and Shelton.[21] Recently, Salek et al.[22] computed frequency-dependent hyperpolarizabilities of pNA at the coupled cluster with singles and doubles (CCSD) level with extended basis sets (aug-cc-pVDZ and a slightly reduced aug-cc-pVTZ), but even at this high level, the computed values differed from the experimental gas-phase values by 25%. Even larger discrepancies were found in comparison with measurements in solution at higher frequencies and were ascribed to experimental errors rather than problems in the computations.

We feel, however, that there are several aspects in the computational procedure and in the comparison with experiments which should be very carefully reexamined. Apart from the usual points as conventions of definition, calibration factors, static correlation effects, and vibrational contributions, there are two points more specifically connected with pNA, that is, the dependence of the properties on intramolecular degrees of freedom and the pertinent geometry of the molecule in the gas phase and in solution. Concerning the latter aspect, geometry optimizations of free pNA with polarized basis sets in general lead to a pyramidalized amino group. However, X-ray structure experiments have shown that in the pNA crystal the amino group is planar, although slightly twisted.[23,24] This structural difference may be due to local field effects, which would then raise the question about the geometry adopted in solutions of different polarities. Because of the dependence especially of the first hyperpolarizability on the conjugation between the amino and nitro groups, this point may be quite relevant in computations of hyperpolarizabilities aiming at an accuracy level of, say, ±10%. Generally, in computational work on the electric properties of pNA, the planar geometry is taken as the reference geometry for computations of electrical properties, irrespective of the phase. On the other hand, computations using self-consistent reaction field models or polarized continuum models have shown that the phase has an important influence on the properties of pNA which cannot be explained by local field effects alone.[25−27]

For similar reasons, the dependence of the properties on internal motions, specifically the torsional motions of the amino and nitro groups and the inversion motion of the amino group, should be examined. Very shallow energy barriers for both torsional modes have been found by Fartzdinov et al.,[28] employing semiempirical methods, and it has been shown that in pNA with orthogonal amino and/or nitro groups the value of the dominant component of β is strongly reduced.[29]

Here, we report on the computation of the structure and the electric properties of the four molecules, of which the systems simulated in quadrupolar approximation will consist, that is, cyclohexane (CH), 1,4-dioxane (DI), tetrahydrofuran (THF), and *p*-nitroaniline (pNA). For pNA, in particular, the structure dependence of the electric properties will be investigated. All the molecular properties necessary for the computation of the permanent local fields in quadrupolar approximation and the macroscopic linear and nonlinear dipole susceptibilities of the pure liquids and the solutions are computed. This includes, for the dipolar properties, frequency dispersion, static as well as dynamic correlation effects, and vibrational contributions, which should be added in the static limit to the electronic properties for the calculation of the permanent local field and at least in the form of the so-called zero-point vibrational average (ZPVA) for the computation of the frequency-dependent values. It has been shown recently that the double perturbation series applied to compute pure vibrational (PV) properties may be not convergent in some cases,[30−32] and we will investigate this point for the four molecules studied here. For pNA, the effect of three large-amplitude motions on the dipolar properties will be investigated by classical averaging. To be able to assess the influence of higher-order terms of the multipolar expansion on the permanent local field, higher-order multipoles up to hexadecapole will be reported, too.

A note on the tensor notation: Tensors of first and second rank are denoted by singly and doubly underlined letters, respectively; tensors of third and fourth rank will be denoted by singly and doubly underlined bold-faced letters.

2. Methods

2.1. Molecular Properties. The multipoles are defined as *n*th moments of the charge distribution $\rho(\underline{r})$[33−36]

$$M^{(n)}_{i_1,\ldots,i_n} = \frac{1}{n!}\int \rho(\underline{r}) r_{i_1}\ldots r_{i_n}\,\mathrm{d}^3 r \tag{1}$$

where $M^{(n)}_{i_1,\ldots,i_n}$ is an element of the multipole moment in Cartesian coordinates, with $M^{(1)} \equiv \mu$ the dipole, $M^{(2)} \equiv Q$ the quadrupole, $M^{(3)} \equiv O$ the octopole, and $M^{(4)} \equiv H$ the hexadecapole moment. All multipole moments and polarizabilities refer to the center of nuclear charge.

The (hyper)polarizabilities are defined as expansion terms of the Fourier components of the total dipole and quadrupole moments according to

$$[\underline{\mu}](\omega) = \underline{\mu}\delta_{\omega^0} + \underline{\underline{\alpha}}^{(11)}(-\omega;\omega)\cdot\underline{E}_\omega + \underline{\boldsymbol{\alpha}}^{(12)}(-\omega;\omega):\nabla\underline{E}_\omega + \frac{1}{2}K^{(2)}_{1,2}\underline{\boldsymbol{\beta}}(-\omega;\omega_1,\omega_2):\underline{E}_{\omega_2}\underline{E}_{\omega_1} + \frac{1}{6}K^{(3)}_{1,2,3}\underline{\boldsymbol{\gamma}}(-\omega;\omega_1,\omega_2,\omega_3):\underline{E}_{\omega_3}\underline{E}_{\omega_2}\underline{E}_{\omega_1} \tag{2}$$

$$\underline{\underline{Q}}(\omega) = \underline{\underline{Q}}\delta_{\omega^0} + \underline{\boldsymbol{\alpha}}^{(21)}(-\omega;\omega)\cdot\underline{E}_\omega + \underline{\underline{\boldsymbol{\alpha}}}^{(22)}(-\omega;\omega):\nabla\underline{E}_\omega \tag{3}$$

where $\underline{E}_\omega$ and $\nabla\underline{E}_\omega$ are Fourier amplitudes of the field and field gradient, respectively, $\underline{\underline{\alpha}}^{(11)}$, $\underline{\boldsymbol{\alpha}}^{(12)}$, $\underline{\boldsymbol{\alpha}}^{(21)}$, $\underline{\underline{\boldsymbol{\alpha}}}^{(22)}$ are the dipole−dipole, dipole−quadrupole, quadrupole−dipole, and quadrupole−quadrupole polarizabilities and $\underline{\boldsymbol{\beta}}$ and $\underline{\boldsymbol{\gamma}}$ are the (dipole) first and second hyperpolarizabilities. The $\underline{\underline{K}}^{(n)}_{\ldots}$ are numerical factors arising from intrinsic permutation symmetry and the factor $^1/_2$ in the definition of the Fourier amplitudes E_ω.[37,38] Note that $\boldsymbol{\alpha}^{(12)}$ and $\boldsymbol{\alpha}^{(21)}$ are related by $\alpha^{(12)}_{\alpha,\beta\gamma} = \alpha^{(21)}_{\beta\gamma,\alpha}$.

Static electrical properties were computed at the MP2 level (density functional theory using the B3LYP functional (DFT/B3LYP) for the higher multipoles and polarizabilities of pNA) with the polarization-consistent Pol basis set, which was developed by Sadlej[39] for the computation of dipole−dipole polarizabilities $\alpha^{(11)}_{ij}$, but has also been used to compute dipole hyperpolarizabilities[13,40,41] and higher-order multipoles and polarizabilities.[10,42] The performance of this basis set was tested for CH, DI and THF by comparison with two larger basis sets from the correlation-consistent basis set series developed by Dunning and co-workers,[43−48] namely, the doubly augmented double-ζ set d-aug-cc-pVDZ, which includes more diffused functions, and the augmented triple-ζ set aug-cc-pVTZ, which contains *f* functions for second-row atoms and *d* functions for H.

For the dominant components of the dipolar (hyper)polarizabilities of pNA, we also employed CCSD(T), MCSCF,[49,50] and multireference SCF with Møller−Plesset second-order perturbation (MRMP2).[51,52] For the active space in the latter calculation,

we followed Luo et al.[3,13] and employed a full π space of orbitals, distributing 12 electrons over 12 π orbitals, 1-8a and 1-4a′ in symmetry group C_s, with one correlating orbital per occupied SCF orbital. For these highly correlated methods, we used a smaller basis developed by Ågren et al.[53] based on Dunning's double-ζ valence basis set, augmented with *d* functions ($\alpha = 0.2$) on C, N, O and with *p* functions on H ($\alpha = 0.1$), abbreviated in the following by D95V(p,d).

Frequency-dependent values of dipole polarizabilities $\alpha_{ii}^{(11)}(\omega)$, $\alpha_{ii}^{(11)}(3\omega)$, and second dipole hyperpolarizabilities $\gamma_{iijj}(-3\omega; \omega, \omega, \omega)$ for CH, DI, and THF as well as $\alpha_{ii}^{(11)}(\omega)$, $\alpha_{ii}^{(11)}(2\omega)$, $\beta_{iij}(-2\omega; \omega, \omega)$ and $\gamma_{iijj}(-2\omega; \omega, \omega, 0)$ for pNA were computed at the random phase approximation (RPA); some (hyper)polarizability components of pNA were also computed at the coupled-cluster level with singles and the contribution of doubles arising from the lowest order in perturbation theory, CC2.[54] The properties $\underline{\boldsymbol{\alpha}}^{(12)}$, $\underline{\boldsymbol{\alpha}}^{(21)}$, $\underline{\underline{\boldsymbol{\alpha}}}^{(22)}$ are computed only for $\omega = 0$.

Finite field techniques as advocated by Cohen and Roothan[55] were applied to obtain the static dipolar properties at the MP2, CCSD(T), and MRMP2 levels using total energies and homogeneous fields, with a base field value of 0.003 au. The higher-order polarizabilities $\underline{\boldsymbol{\alpha}}^{(12)}$ and $\underline{\underline{\boldsymbol{\alpha}}}^{(22)}$ were computed similarly from dipole and quadrupole moments with applied first field gradients, using a base value of 0.0005 au.[34] [Note: The values of the field gradients were *halved* in the input for *Gaussian 98*, to be consistent with the conventions used here. Similarly, second and third field gradients should be divided by 6 and 24, respectively. This may be checked by comparing the higher multipoles computed by *Gaussian 98* with corresponding values computed from finite differences of energies with applied field gradients. Note that the multipoles in the output file of *Gaussian 98* are defined as *n*th-order moments of the charge density; the relationship to the moments $M^{(n)}$ defined in eq 1 is $M^{(n)\mathrm{G98}}_{i_1,\ldots,i_n} = n!M^{(n)}_{i_1,\ldots,i_n}$.] In both cases, calculations with a base value two times larger gave only negligibly different properties. Comparison of the diagonal values $\alpha_{ii,jj}^{(22)}$ obtained by finite field differences from in-field gradient *quadrupole* values with those obtained using in-field gradient *energies* showed that the nonvalidity of the Hellmann−Feynman theorem for MP2[56] did not affect the computed values.

Most of the molecular calculations were done with *Gaussian 98*,[57] except for frequency-dependent computations, for which the program Dalton[58] was employed, and the MRMP2 computations, which were done with GAMESS.[59]

Vibrational Contributions. For all the molecules, we computed zero-point vibrational average (ZPVA) and pure vibrational (PV) contributions to the dipolar properties in the framework of Bishop−Kirtman perturbation theory (BKPT).[60] ZPVA contributions are known to follow a similar dispersion behavior as the electronic contribution[60] and may therefore be important for optical and static susceptibilities. PV contributions are usually very small for applied fields with only optical frequencies and may therefore be neglected at optical frequencies, but should be taken into account for static properties, which determine, for example, the local fields in the material.

Static ZPVA and PV terms were calculated at the restricted Hartree−Fock (RHF) level with the 6-311G** basis set for CH, DI, and THF and with 6-31G** for pNA, with the geometries optimized at the same level and basis set. To compute the necessary derivatives, the numerical differentiation scheme with finite fields and geometry displacements described in ref 61 was used. This method allows the computation of the third derivative of the energy with respect to normal coordinates and the first and second derivatives of μ, α, β, and γ with respect to normal coordinates. With these derivatives, the ZPVA contribution can be computed up to the first order both in electrical and mechanical anharmonicity in the double perturbation expansion applied in BKPT. As the numerical scheme applied does not allow to compute frequency-dependent values, the ZPVA values were multiplicatively scaled with the electronic dispersion to obtain estimates at the frequency-dependent level.

In the case of the PV contributions, the available derivatives allow a computation of all terms of the so-called double harmonic approximation (DH), of order 0 in both anharmonicities, as well as the next higher-order term in the double perturbation series for $\alpha^{(11)}$, β, and γ, which is of order 1 in one of the anharmonicities and of order 0 in the other. It also allows the computation of some, but not all, terms of the next expansion term, where the sum of the two anharmoncity orders add up to 2. As it does not seem to be consistent to use only a partially computed expansion term, we adopted the following procedure: if the sum of the higher-order terms was small compared with the terms at the DH approximation, we assumed that the perturbation series converges rapidly and considered the DH values a valid approximation to the PV values; if this condition was not fulfilled, we assumed that the expansion may not converge and discarded the PV contributions. This procedure has been inspired by several reports in the literature which show that the double perturbation expansion in some cases may be not even initially convergent.[30−32]

To check for correlation effects, an additional computation of the vibrational properties of pNA at the B3LYP/6-311G** level was performed. In this case, no second derivatives of β and no derivatives of γ were available. Therefore, to be directly comparable with the RHF properties, only PV contributions of α and β and ZPVA contributions of α were computed. For CH, DI, and THF, vibrational contributions at the double harmonic level were also computed at the MP2 level.

Results and Discussion

Geometry of pNA. An accurate description of the geometry of NH_3 and other compounds containing amino groups is known to depend critically on polarization functions on nitrogen.[62−64] In pNA, the amino group may be pyramidalized as in aniline or planar, due to more favorable conjugation effects in this geometry. To investigate this, the gas-phase geometry of pNA was optimized at the MP2 level using several basis sets: 6-31G**, 6-311G**, cc-pVDZ, cc-pVDZ with aug-cc-pVDZ on N (cc-pVDZ+aug-cc-pVDZ(N)), aug-cc-pVDZ, cc-pVTZ, cc-pVTZ+aug-cc-pVTZ(N). In all occasions, the final geometry was of C_s symmetry, although only for the smaller double-ζ basis sets could it be established that the stationary point is in fact a minimum, as the aug-cc-pVDZ and the triple-ζ basis sets were too large to compute the Hessian. The amino group is always pyramidalized, as evidenced by the torsional angle H−N−C−C shown in Table 1, in accord with previous optimizations of pNA using different polarized and/or diffused basis sets of the 6-31 family, for example, in ref 65. To decide on the geometry to be used for our calculations, we computed the dipolar electric properties with each geometry at the MP2/D95V(p,d) level. The results given in Table 1 clearly demonstrate the importance of polarized functions in the *geometry optimization* for the electrical properties of pNA: the properties change continuously in the double-ζ series cc-pVDZ, cc-pVDZ+aug-cc-pVDZ(N), aug-cc-pVDZ and similarly in the triple-ζ series cc-pVTZ, cc-pVTZ+aug-cc-pVTZ(N) (the fully

TABLE 1: Influence of Basis Set and Correlation Employed in the Geometry Optimization on Torsional Angle H−N−C−C (ψ_{NH_2}/deg) and on the Dipolar Electrical Properties of PNA, Computed at the MP2/D95V(p,d) Level[a]

geometry	ψ_{NH_2}	μ	$\alpha_{av}^{(11)}$ [b]	β_{xxx}	γ_{av} [c]
6-31G**/MP2	27.6^0	2.376	100.28	1639.6	28.9
6-311G**/B3LYP	19.2^0	2.512	100.45	1650.2	28.2
cc-pVDZ/MP2	29.4^0	2.297	100.50	1468.8	27.2
cc-pVDZ+aug-ccpVDZ(N)/MP2	27.4^0	2.325	100.77	1520.7	27.6
aug-cc-pVDZ/MP2	25.8^0	2.382	101.54	1623.2	28.9
cc-pVTZ/B3LYYP	19.3^0	2.512	99.97	1638.9	28.1
cc-pVTZ/MP2	26.2^0	2.353	99.04	1506.1	27.1
cc-pVTZ+aug-ccpVTZ(N)/MP2	25.1^0	2.373	99.25	1532.8	27.4

[a] Only average values shown, except for β, where the dominant component is given. γ in 1000 au; all other units in au. [b] $\alpha_{av}^{(11)} = {}^1/_3\Sigma_i\alpha_{ii}^{(11)}$. [c] $\gamma_{av} = {}^1/_{15}\Sigma_{ij}(\gamma_{iijj} + \gamma_{ijij} + \gamma_{ijji})$.

augmented basis could not be employed due to restricted computer resources). The similarity of the trends for the two basis sets suggests that the full aug-cc-pVTZ basis may yield similar properties to those of aug-cc-pVDZ. On the other hand, all fully polarized basis sets yield very similar properties at the MP2 level, which we thus consider to be converged. Considering the absence of the Hessian for the larger basis sets, we finally employed the MP2/6-31G** optimized geometry for our computations. The B3LYP optimized geometries with basis 6-311G** and cc-pVTZ are very similar and yield very similar electrical properties. Although the geometries are slighly different from the MP2 optimized ones, they still yield similar electrical properties as the MP2 geometries optimized with fully polarized basis sets.

Starting the gas-phase optimization from a geometry of C_1 symmetry, with both the nitro and amino groups nearly orthogonal to the phenyl plane, leads back to a geometry of C_s symmetry, indicating that there is no lower geometry with a *twisted* substituent group.

Finally, we considered the effect of static correlation on the optimized gas-phase geometry. Mikkelsen et al.[3] reported that static correlation effects have a considerable effect on the electronic ground state of pNA due to the biradicaloid character of the nitro group. A stability analysis of the RHF/Pol wave function indeed shows that the wave function has a singlet RHF → UHF instability, indicating a singlet biradicaloid ground state.[66] We therefore reoptimized the isolated molecule at the MCSCF/6-31G** level, employing as the active space the full π orbital space as described in section 2, to investigate if inclusion of static correlation would lead to a more stable geometry of C_{2v} symmetry in the isolated state. Computer memory restrictions did not allow computation of the Hessian for this large system; therefore, two optimizations were carried out, constraining the molecular symmetry either to C_s or to C_{2v}. The stationary geometry reached in the C_s group was still considerably nonplanar (torsion angle H−N−C−C = 25.98°), and had a considerably lower total energy than the planar stationary geometry (−489.375 au versus −489.355 au, corresponding to an energy difference of 52.5 kJ/mol), which probably is a transition state. Thus, it appears that, at the MCSCF level also, the nonplanar geometry of pNA is more stable than the planar one in the isolated state.

Contrary to the results obtained here, the amino group of pNA in the crystal is *planar*, although the plane is not coplanar with the plane of the phenyl ring, possibly due to the hydrogen-bonding network.[23,24] This is, to our knowledge, the only experimental information available about the geometry of pNA. It has been used as justification to assume that pNA adopts C_{2v} symmetry in solution and in the gas phase.[3,12] To investigate if this discrepancy between ab initio and crystal geometry may be caused by the strong local field acting on the molecules, we reoptimized the pNA molecule at the B3LYP level, applying additionally several different continuum solvation or self-consistent reaction field (SCRF) models: the method according to the spherical Onsager model (OSCRF), the polarizable continuum model in the integral equation formalism (IEF-PCM),[67] the self-consistent isodensity polarized continuum model (SCIPCM),[96] and the conductor-like sreening model (COSMO) model in the formulation of Barone and Cossi (BC-COSMO).[68] The default settings for the solvent THF were applied in all cases. The 6-311G** basis was employed for all models, and the Hessian was computed to confirm that an extremal point on the potential surface had been found. For comparison, some models were also tried with the cc-pVTZ and aug-cc-pVDZ basis sets, without computing the Hessian. Table 2 shows the torsional angle H−N−C−C and the dipolar electric properties obtained at the D95V(p,d) level for the different SCRF basis set combinations.

TABLE 2: Torsional Angle ψ_{NH_2}/deg and Dipolar Electric Properties at the MP2/D95V(p,d) Level, Computed for Geometries Optimized with Different Continuum Solvation Models and Basis Sets at the B3LYP Level[a]

solv. model	basis	ψ_{NH_2}	μ	$\alpha_{av}^{(11)}$	β_{xxx}	γ_{av}
BC-COSMO	6-311G**	12.9^0	2.671	101.8	1848	29.6
SCIPCM	6-311G**	12.6^0	2.693	102.1	1884	29.9
	cc-pVTZ	9.8^0	2.724	101.9	1894	29.6
IEFPCM	6-311G**	12.6^0	2.674	101.8	1847	29.6
	cc-pVTZ	9.2^0	2.760	102.5	1949	29.8
	aug-cc-pVDZ	7.3^0	2.741	103.3	1991	30.8
OSCRF	6-311G**	0.1^0	2.763	102.7	1946	30.3
	cc-pVTZ	0.1^0	2.769	102.2	1935	30.0

[a] γ in 1000 au; all other units in au.

Starting from the gas-phase MP2/6-31G** optimized geometry, the SCRF optimizations lead to geometries with reduced nonplanarity; in the case of the OSCRF model, the geometry is nearly planar, independent of the basis. The more sophisticated SCRF models all predict nonplanar geometries, but with increasing basis sets, the torsional angle decreases. The electric properties are only slightly dependent on the solvation model and basis set employed, with the largest difference of 8% found for β_{xxx}. Discarding the IEFPCM/6-311G** and BC-COSMO/6-311G** models, the largest difference decreases to 5%. Considering the observed trends of the properties and torsional angles as well as the availability of the Hessian, we chose the OSCRF/6-311G** optimized geometry as the basis for our computations.

We mention that with the OSCRF/6-311G** model a similar minimum with near-C_{2v} symmetry as obtained for the solvent THF was found for other values of the dielectric constant ϵ_r in the range $\epsilon_r = 4-40$. If dielectric constants corresponding to nonpolar solvents ($\epsilon_r = 2-3$) were applied, however, the optimization led again to a pyramidalized amino group, similar to that of the gas phase. We conclude that the local field acting on the pNA molecule in polar solvents causes geometry changes which, as we will show below, lead to substantially different electrical properties compared to those of the molecule in the gas phase and in nonpolar solvents.

We note that the gas-phase optimization of pNA with basis sets without polarized functions, as 6-31G or the Dunning basis set D95V, leads to optimum structures with C_{2v} symmetry, which has sometimes been exploited to assume that this is in fact the optimized structure of pNA independent of the

TABLE 3: Static Electrical Properties of pNA Computed with Different Methods and Basis sets [I = Pol, II = D95V(p,d)][a]

	gas		solution $\epsilon_r = 7$					
geom	MP2/I	CC2/II	MP2/I	MP2/II	CCSD(T)/II	MCSCF/II	MRMP2/II	CC2/II
μ_x, μ_z	2.378, 0.387		2.799, 0.001	2.763, 0.001	2.792, −	2.460, −	2.740, −	
$\alpha_{ii}^{(11)}$	152.06, 105.19, 56.86	153.85, −	159.46, 105.03, 56.87	153.99, 102.86, 51.17	150.93, −	128.98, −	147.59, −	160.96, −
$\alpha_{av}^{(11)}$	104.70	104.81	107.12	102.67				
β_{xii}	1646.1, −50.0, −50.1	1818.5, −	1954.6, −72.7, −62.7	1945.7, −74.2, −37.1	1981.8, −	1412.0	2091.4, −	2124.7, −
$\beta_{\|\|}$[b]	913.3		1091.5	1100.6				
γ_{iiii}	144.2, 11.4, 10.7	197.8, −	152.9, 11.1, 11.9	144.8, 6.6, 1.5	165.0, −	159.1, −	250.7, −	212.6, −
γ_{iijj}	−0.4, 5.6, 6.0		−1.8, 6.4, 6.2	−3.7, 1.3, 1.8				
γ_{av}	37.8		39.5	30.3				

	gas		solution $\epsilon_r = 7$	
geom	B3LYP/I	MP2/I	B3LYP/I	B3LYP/II
Q_{ii}	−22.5, −19.9, −22.2	−22.8, −	−21.1, −20.1, −23.0	−21.2, −20.0, −22.3
O_{iix}	19.5, 3.5, −2.7	17.0, −	22.9, 3.5, −3.3	25.2, 4.0, −3.0
H_{iiii}	−164, −41, −7	−167, −	−150, −42, −8	−157, −41, −7
H_{ijij}	−34, −30, −9		−33, −33, −8	−34, −30, −9
$\alpha_{x,ii}^{(12)}$	108.7, −7.5, 3.9	108.9, −	112.2, −7.5, 3.7	120.1, −6.9, 4.7
$\alpha_{i,xi}^{(12)}$	108.7, 13.7, 24.7		112.2, 14.6, 23.4	120.1, 16.5, 19.6
$\alpha_{ii,ii}^{(22)}$	1425, 367, 74	1412, −	1436, 371, 74	1335, 357, 51
$\alpha_{jj,ij}^{(22)}$	−88, 2, 6		−91, 1, 6	−82, −5, 4.0
$\alpha_{ij,ij}^{(22)}$	516, 279, 109		513, 274, 109	491, 228, 91

[a] The index *i* runs over *x*, *y*, and *z*, and the double index *ij* runs over *xy*, *xz*, and *yz*; γ in 10^3 au and all other units in au. [b] $\beta_{\|\|} = (1/5|\mu|)\,\Sigma_{ij}(\beta_{iij} + \beta_{iji} + \beta_{jii})\mu_j$.

phase.[69,70] Our calculations show, however, that the real situation may be more complicated. We also note that previous workers[25−27] already reported a strong influence of the solvent on the electric dipolar properties of pNA and other molecules, using the SCRF method at the RHF/6-31G* and the semiempirical AM1 level, but did not analyze the reason in terms of geometry changes. A similar solvent-induced geometry change of the amino group of cytosine tautomers in acetonitrile solution has recently been reported by Alparone et al.[71]

To our knowledge, there is no experimental investigation concerning the geometry of pNA in the gas phase or in solution. Unfortunately, vibrational Raman and IR measurements cannot resolve the matter, because the vibrational frequencies predicted by DFT/B3LYP together with polarized basis sets for the gas-phase geometry and for the near-planar solution-phase geometry are nearly identical, and both coincide well with measured solution-phase spectra.[72,73] The insensitivity of the vibrational frequencies of Raman-active modes on the polarity of the solvent has been observed experimentally.[74] The only mode which differs considerably between the two optimized geometries is the amino wagging mode, found at 363 cm^{-1} in the B3LYP/6-311G** gas-phase geometry and at 165 cm^{-1} in the geometry predicted by OSCRF/B3LYP/6-311G** for polar solvents. Neither band has been observed in Raman or IR spectra conducted in polar solvents.[72,73] We should note that the vibrational frequencies computed at the MP2/6-31G**//MP2/6-31G** level differ considerably from those obtained at the B3LYP/6-311G**//B3LYP/6-311G** level.

Electronic Properties of pNA. A compilation of the computed static properties of pNA is given in Table 3, with the employed coordinate system shown in Figure 1. For the free molecule, results obtained for the MP2/6-31G** geometry are shown; values computed at the B3LYP/6-311G** geometry at the RPA/Pol level were very similar (e.g., $\alpha_{av}^{(11)} = 98.49$ au, $\beta_z = 1142$ au at $\lambda = 1064$ nm for the MP2/6-31G** geometry, and $\alpha_{av}^{(11)} = 98.81$ au, $\beta_z = 1178$ au for the B3LYP/6-311G** geometry).

Concentrating first on the comparison of different basis sets and computational levels carried out with the B3LYP/OSCRF/6-311G** geometry, we see in the MP2/Pol and MP2/D95V(p,d) results up to β that both basis sets give nearly identical values, in agreement with the claim of Ågren et al.[75] that D95V(p,d) yields results close to the basis set limit. For γ, however, Pol gives slightly larger values than D95V(p,d), especially for the diagonal components in directions perpendicular to the dipole axis, which indicates that D95V(p,d) is not flexible enough in these directions for high-order properties. Differences of similar magnitude are found for the higher-order polarizabilities, computed at the computationally less expensive DFT/B3LYP level. As a test for the accuracy of this level, we also computed the diagonal component in the *x*-direction of the multipoles and higher-order polarizabilities at the MP2 level for the gas-phase geometry. The MP2 values differ only by a few percent from the corresponding DFT values, except for O_{xxx}, where the difference is within ∼10%, still acceptably small. The higher correlated methods CCSD(T) and MRMP2 with the D95V(p,d) basis give similar results for the diagonal components of the dipolar properties in the dipole axis direction as MP2/D95V(p,d) for μ_x, α_{xx}, and β_{xxx}. For γ_{xxxx}, however, MCSCF/D95V(p,d) gives a similar value as MP2/D95V(p,d) and CCSD(T)/D95V(p,d), while the value obtained with MRMP2/D95V(p,d) is 73% larger than the MP2/D95V(p,d) value. This indicates that static correlation is very important for this property and the MP2/Pol values may only be approximately correct. Finally, comparison of the CC2/D95V(p,d) and CCSD(T)/D95V(p,d) results show that CC2 overshoots the CCSD(T) values for β_{xxx} and γ_{xxxxx} considerably. Similar overestimations of the CC2 method have been reported earlier.[61,76]

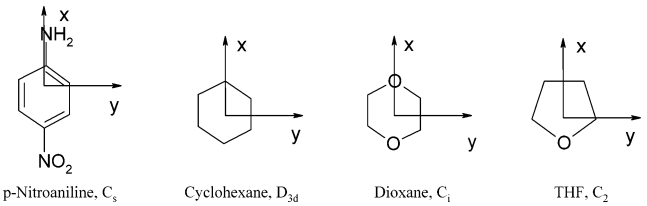

Figure 1. Structural formulas, molecular coordinate systems, and symmetry groups of cyclohexane (CH), 1,4-dioxane (DI), tetrahydrofuran (THF), and *p*-nitroaniline (pNA).

TABLE 4: Frequency-Dependent Dipolar Electrical Properties $\alpha^{(11)}(-2\omega; 2\omega)$, $\beta(-2\omega; \omega, \omega)$, and $\gamma(-2\omega; \omega, \omega, 0)$ at $\lambda = 2\pi/(hc\omega) = 1064$ nm of PNA Computed at the RPA/Pol, CC2/D95V(p,d), and (scaled MP2)/Pol Levels for the MP2/6-31G and the B3LYP/OSCRF/6-311G** Geometries[a]**

	gas		solution $\epsilon_r = 7$	
geom.	RPA	Sc. MP2	RPA	Sc.MP2
$\alpha_{ii}^{(11)}$	150.55, 104.56, 55.84	167.34, 110.33, 58.24	162.64, 106.33, 55.55	178.45, 110.63, 58.27
$\alpha_{av}^{(11)}$	103.65	111.97	108.17	115.78
β_{xii}	1397.9, −228.0, −41.1	2228.5, −62.7, −58.2	1793.4, −297.0, −42.7	2714.9, −93.3, −73.4
β_{iix}	1397.9, −208.6, −40.2	2228.5, −57.4, −56.9	1793.4, −270.8, −42.1	2714.9, −85.1, −72.3
$\beta_{\|\|}$	675.4	1254.8	882.8	1532.6
γ_{iiii}	109.6, 11.5, 10.3	208.1, 13.1, 12.1	131.0, 11.9, 10.7	230.4, 13.0, 13.5
γ_{iijj}	−1.4, 4.3, 5.4	−1.4, 6.8, 7.2	−3.1, 5.0, 5.6	−3.7, 8.0, 7.4
γ_{ijji}	−2.4, 4.1, 5.4	−2.4, 6.5, 7.1	−4.7, 4.7	−5.7, 7.5, 7.3
γ_{jjii}	−0.6, 4.1, 5.3	−0.6, 6.5, 7.0	−2.0, 4.8, 5.5	−2.5, 7.7, 7.2
γ_{jiij}	−1.9, 4.0, 5.3	−1.9, 6.4, 7.0	−4.0, 4.6, 5.5	−4.8, 7.4, 7.2
γ_{av}	29.5	51.6	33.6	55.9
	CC2	Sc. MP2	CC2	Sc.MP2
α_{xx}	173.93	171.91	185.33	183.60
α_{av}	113.67	113.55	117.39	117.49
β_{xxx}	2807.8	2541.7	3366.2	3096.7
γ_{xxxx}	349.0	254.4	393.3	282.9
$\langle\gamma\rangle_E$	calcd 720[b], 750[c]	exptl[d] 710 ± 20		

[a] γ in 10^3 au; all other properties in au. [b] $\langle\gamma\rangle_E = \mu\beta_{\|\|}/3kT + \gamma_{av}$, using MP2/Pol values scaled by RPA dispersion. [c] $\langle\gamma\rangle_E = \langle\mu\beta_{\|\|}\rangle_\Omega/3kT + \langle\gamma_{av}\rangle_\Omega$, using CC2 dispersion and torsional averaging, see text. [d] Ref 15, $T = 470.05$ K.

Comparison of the MP2/Pol results for the MP2/6-31G** gas-phase geometry and the OSCRF/B3LYP/6-311G** geometry shows that the local field induced geometry change increases μ and $\beta_{\|\|}$ by 16% and 20%, respectively, while the corresponding changes of $\alpha^{(11)}$, γ, and the higher-order polarizabilities are small. The frequency-dependent dipolar (hyper)polarizabilities corresponding to EFISH at $\lambda = 1064$ nm at the RPA level given in Table 4 show that the solvent-induced change increases for $\beta_{\|\|}(-2\omega; \omega, \omega)$ slightly to 22%. The dispersion computed at the RPA level is probably underestimated, as indicated by the first allowed electronic excitation, predicted by RPA/Pol for the gas-phase geometry to be at $\lambda = 246$ nm, while experimentally, it is found at $\lambda \approx 290$ nm.[77,78] At the more highly correlated CC2 level, a stronger dispersion is found, in particular for β_{xxx}, for which the dispersion increases from 35.4% at the RPA level to 54.4%, and γ_{xxxx}, for which it increases from 44.3% to 76.0%. However, CC2 still overestimates the first allowed excitation energy ($\lambda = 271$ nm). We note that the same value is obtained for the B3LYP/6-311G** optimized geometry. To check for the influence of higher correlation, a computation on the CCSD level was performed. This *increases* the excitation energy ($\lambda = 261$ nm). This indicates first that the dispersion of β computed at these highly correlated levels may still be slightly underestimated and second that the *dispersion* at the CC2 level may be more accurate than that at the CCSD level. However, due to the overestimation of the *static* properties of CC2 mentioned above, the CC2 dispersion should only be used to scale the more reliable static values, for example, MP2/Pol.

For the B3LYP/OSCRF/6-311G** optimized geometry, the predicted excitation energies are lower than for the gas-phase geometry (CC2, $\lambda = 279$ nm; CCSD, $\lambda = 271$ nm), resulting in an *geometry-induced* increased dispersion with respect to the gas-phase geometry for β_{xxx} to 58.4% and γ_{xxxx} to 85.0%.

In Table 5, we show the results of an analysis of the reason for the difference of μ and β_{xxx} between the gas- and solution-phase geometries in terms of structural parameters, computed at the RHF/D95V(p,d) level. The properties were computed for several structures, starting from the gas-phase structure and successively replacing individual structure parameters by those occurring in the solution-phase geometry. In this way, three relevant parameters were identified: the pyramidalization of the amino group and the two C−N bond lengths. As shown in Table 5, the pyramidalization of the amino group has the largest influence on the change of μ and β_{xxx}: it induces 40−60% of the overall change of the properties between the two geometries, while the two bond lengths cause changes between 3% and 30%. All three parameters together account for nearly 100% of the change in β_{xxx} and for 80% of the change in μ.

TABLE 5: Evolution of μ and β_{xxx} of the Gas-Phase Structure (GS) of pNA toward the Values of the Solution-Phase Structure (SS) by Successively Replacing Individual Structure Parameters[a]

base geometry	NH_2 pyramidal	r_{C-NO_2}[b]	r_{C-NH_2}[c]	μ	β_{xxx}
GS	GS	GS	GS	2.784	1031
GS	SS	GS	GS	2.979	1155
GS	SS	SS	GS	2.989	1199
GS	SS	SS	SS	3.100	1234
SS	SS	SS	SS	3.182	1242

[a] Properties computed at the RHF/D95V(p,d) level. [b] $r_{C-NO_2} = 1.462$ Å (GS), 1.448 (SS). [c] $r_{C-NH_2} = 1.394$ Å (GS), 1.356 (SS).

The dipolar electronic properties of pNA obtained here are comparable with those of several previous studies applying comparable basis sets, geometries, and computational levels,[3,12,14,79] except for the DFT-based methods,[14,79] which predict a much larger dispersion for β than RPA and MCSCF methods.

Our best value of $\beta_{xxx}(-2\omega; \omega, \omega)$ at $\lambda = 2\pi hc/\omega = 1064$ nm (3097 au) for the B3LYP/OSCRF/6-311G** geometry is 7.4% larger than the corresponding CCSD/aug-cc-pVDZ value (2882 au) obtained by Salek et al.,[22] who used the experimental crystal geometry but with the amino group rotated to yield C_{2v} symmetry. This difference is nearly entirely accounted for by the different dispersion of CC2 and CCSD: scaling our MP2/Pol value with the CCSD dispersion factor of ref 22 (1.5018) yields 2935 au, which differs only by 1.9% from their CCSD/aug-cc-pVDZ value. This indicates that neither the basis set nor the employed geometry have an influence on β_{xxx} which is yet unaccounted for in our calculations. As discussed above, CCSD may still underestimate the correlation effect on the dispersion.

We finally note that Salek et al. also used a stripped-down version of the aug-cc-pVTZ basis set and obtained very similar values for the first hyperpolarizability $\beta_{\|\|}$ as with the aug-cc-

TABLE 6: Static PV and ZPVA Contributions to the Dipolar (hyper)Polarizabilities of pNA[a]

	PV	ZPVA		PV	ZPVA		PV	ZPVA
				RHF/6-31G**				
$\alpha_{xx}^{(11)}$	50.1 (186.2)	3.10	β_{xxx}	1674 (8354)	3.2	γ_{xxxx}	115.4 (6478)	
$\alpha_{yy}^{(11)}$	9.7 (33.3)	2.21	β_{xyy}	−56 (1154)	2.3	γ_{yyyy}	0.9 (274)	0.15
$\alpha_{zz}^{(11)}$	30.5 (141.4)	0.96	β_{xzz}	−8 (6319)	0.5	γ_{zzzz}	−0.1 (6568)	0.00
			β_{zzz}	−169 (5802)	0.6	γ_{xxyy}	5.0 (857)	0.03
			β_{zxx}	402 (−1674)	−6.7	γ_{xxzz}	0.8 (6207)	0.00
			β_{zyy}	28 (−404)	−1.5	γ_{yyzz}	0.2 (404)	0.02
				B3LYP/6-311G**				
$\alpha_{xx}^{(11)}$	55.8 (235.6)	3.67	β_{xxx}	1998 (8963)		β_{zzz}	−148 (7625)	
$\alpha_{yy}^{(11)}$	6.5 (21.0)	2.77	β_{xyy}	−18 (1018)		β_{zxx}	405 (7780)	
$\alpha_{zz}^{(11)}$	31.9 (185.2)	0.95	β_{xzz}	8 (7682)		β_{zyy}	43 (−321)	

[a] Computed at the double harmonic (DH) level, numbers in brackets show PV contributions including some terms of higher-order expansion; see text. Vibrational contributions computed at the RHF/6-31G** and B3LYP/6-311G** levels; $\alpha^{(11)}$, β in au and γ in 10^3 au.

pVDZ basis set (1316 au versus 1333 au). This indicates that the electric properties obtained here are already converged with respect to basis set expansion.

Vibrational Contributions to the Dipolar Properties of pNA in the Gas Phase. The computed static vibrational contributions of pNA to $\alpha^{(11)}$, β, and γ are shown in Table 6. The ZPVA contributions are so small compared to the electronic properties that they may be neglected. According to the procedure explained in section 2.1, no component of the PV contributions can be considered to be converged at the DH level. For the components of $\underline{\boldsymbol{\beta}}$, the largest contributions are due to the next higher level of perturbation theory, which is of order 1 in either mechanical or electrical anharmonicity and order 0 in the other. Thus, they may be converged at this level. For $\alpha^{(11)}$ and $\underline{\underline{\gamma}}$, however, it is the level of overall anharmonicity order 2 which contributes the largest value; additionally, the more complete PV values are, for some components, so large that they cannot be considered to be credible. This holds for the values computed at both the RHF/6-31G** and B3LYP/6-311G** levels. Generally, the B3LYP/6-311G** values are comparable to those computed at the RHF/6-31G** level. This indicates that correlation effects on vibrational contributions are not so large as to alter the qualitative picture gained at the RHF level. Although one may doubt that DFT in combination with B3LYP captures a significant part of the correlation effect on electric properties, this method is more reliable in computing the vibrational frequencies than RHF and MP2,[80] which are essential ingredients for the vibrational properties. It should also be mentioned that the serious problems encountered for the electric properties of elongated chains computed with DFT in combination with conventional functionals[81−85] do not appear to play a role in pNA.

The main cause for the very large PV values is the vibration involving the amino group wagging motion, predicted at 483.8 cm^{-1} at the RHF/6-31G** level. This can be checked by shifting the frequency of this normal mode artificially to a very high value. Then, the contributions of the corresponding derivatives with respect to this mode are suppressed, as can be seen from the constituting equations, for example, in refs 60 and 86. Using this procedure for the RHF/6-31G** values, most of the PV values become much more reasonable; for example, the series of components β_{xxx}, β_{xyy}, and β_{xzz} in DH approximation are equal to 886, −9, and 57 au, and including higher-order terms, they are equal to 1242, −234, and 19 au, but some components are still very large, for example, $\gamma_{zzzz} = 34.3\ (223.4)\ 10^3$ au.

It cannot be excluded that the missing terms of the higher-order terms for the PV contributions, which are those that involve the fourth derivative of the energy and third-order derivatives of μ and α,[60,86] would cancel the large terms to a great extent, as this could not be checked with the numerical differentiation method employed. We also note that the conclusion of no convergence of the perturbation series holds only for the C_s geometry as obtained from the RHF/6-31G** and B3LYP/6-311G** optimizations; it cannot simply be extended to the solvated structure with approximately C_{2v} symmetry, nor to the structure obtained with the correlated MP2 method. Concerning the effect of correlation, we note that the problematic wagging mode found at 483.8 cm^{-1} with a high IR intensity (452.8 KM mol^{-1}) in the RHF/6-31G** geometry shifts to higher frequency (624.2 cm^{-1}) and lower IR intensity (353.9 KM mol^{-1}) in the MP2/6-31G** structure, which both could lead to a smaller contribution of this mode to the PV terms (the normal frequencies occur in the denominators of these terms, while the IR intensity is determined by the first derivative of μ with respect to the normal vibration coordinates). We note again, however, that the frequencies computed at the B3LYP level are in better accord with experiment than those obtained at the MP2 level,[73] which means that, even if PV contributions at the MP2 level differ from those computed here, they are not necessarily more correct.

In the B3LYP/OSCRF/6-311G** structure, the IR intensity is even lower (236.9 KM mol^{-1}), but the frequency becomes much *smaller* than for the RHF/6-31G** structure (165.6 cm^{-1}). It is not clear a priori how the two opposing trends affect the PV terms, although it has been reported[27] that solvation computed at the RHF/OSCRF/6-31G level increases the PV contribution to β_{xxx} at the DH approximation in CH_3Cl and water considerably. We finally note that our values at the DH level compare reasonably well with those obtained by Champagne[69] and Luis et al.[87] at the RHF/6-31G level, despite the different basis sets and symmetry (6-31G leads to C_{2v} symmetry for pNA).

Conformation Dependence of the Dipolar Properties of pNA in the Gas Phase. The computation of vibrational properties according to BKPT in the last section assumes that anharmonicities of the vibrational motions are small and can be treated by perturbation theory. This is not necessarily a valid assumption for the low-frequency large-amplitude torsional and inversional modes (LAM) of the amino and nitro groups in pNA. Although a treatment of vibrational optical properties going beyond the assumptions in BKPT by applying the vibrational self-consistent field (VSCF) method has recently been developed by Torrent-Sucarrat et al.,[88] this method is still too costly for a large system such as pNA. We thus investigated the influence of conformation of pNA on the dipolar properties on a purely *classical* approximation by computing the thermal average of

the dipolar electric properties over the potential energy surface corresponding to the LAM.

The two possible large-amplitude torsional motions of the amino and nitro groups and the inversion or wagging motion of the amino group were taken into account. The NO_2 torsion is considered to be the mode with the lowest frequency in pNA; its frequency has been estimated to occurr at 57 cm^{-1} in the crystal.[23] The NH_2 wagging and torsion modes are in harmonic approximation predicted to be quite close at 350−400 cm^{-1}.[73] These modes change the conjugation between the acceptor and donor groups, with a possibly considerable influence on the electric properties. A theoretical study at the semiempirical SAM1 level by Fartzdinov et al.[28] found that a broad distribution of twist and wagging angles already exists at low temperatures, while DFT calculations of the energy as a function of the two torsional angles by Chen and Chen[65] suggest a higher energy barrier, indicating that the distribution of twist angles at ambient temperature may be smaller than those predicted by the semiempirical SAM1 method, but still not negligible. Additionally, a strong reduction of the absolute values of μ and β in conformations with orthogonal nitro and amino groups has been reported at the RHF level by Velders et al.;[29] similar distortion effects on γ_{xxxx} have been reported by Yamada et al.[89]

The NO_2 torsion was defined by the dihedral angle ϕ_{NO_2} = O—N—C—C; for the definition of the NH_2 inversion and torsion, we introduced three dummy atoms X_i, $i = 1, 2, 3$, in the MP2/6-31G** optimized geometry, X_1 perpendicular to the N—C bond, such that the dummy atom passes through the N atom when operated upon by the symmetry σ plane, X_2 in a linear prolongation of the C—N bond, and X_3 in the symmetry plane and bisecting the H—N—H angle. The inversion angle was then defined by the dihedral angle $\tau = X_3—X_2—X_1—N$ and the torsion by the dihedral $\phi_{NH_2} = C—C—N—X_1$.

Energies were computed for structures with either ϕ_{NO_2} or τ and ϕ_{NH_2} fixed, while all other coordinates were optimized at the MP2/6-31G** level. The angle ϕ_{NO_2} was incremented by 10° in the interval [0.800°, 180.800°]; τ and ϕ_{NH_2} were changed by 20° covering the intervals [−82.64°, 57.36°] and [2.77°, 182.77°], respectively. For each of the obtained partially optimized geometries, dipolar properties were computed at the MP2/D95V(p,d) level. The obtained energies and properties were fitted to

$$P(\phi_{NO_2}) = \sum_{n=0}^{3} a_n \cos 2n\phi_{NO_2} \quad (4)$$

$$P(\tau, \phi_{NH_2}) = \sum_{n=0}^{3}\left(\sum_{i=0}^{2} b_{ni}\tau^{2i}\right) \cos 2n\phi_{NH_2} \quad (5)$$

where a_n and b_{ni} are fit coefficients and $P = \Delta E$, $|\mu|$, $\alpha_{av}^{(11)}$, $\beta_{||}$, γ_{av}, with ΔE the energy difference with respect to the minimum structure, and the angles are measured in radians. Accurate fits were obtained; the largest percentage deviation of the fits from the computed values, defined by $\Delta P = [\Sigma i(P^{fit}(\Omega_i) - P^{calc}(\Omega_i))^2/\Sigma i(P^{calc}(\Omega_i))^2]^{1/2} \times 100$, ($\Omega = \phi_{NO_2}$ or $\Omega = (\tau, \phi_{NH_2})$) was 1.6% for $P(\Omega) = \Delta E(\tau, \phi_{NH_2})$. The obtained fit coefficients for the relative energies are shown in Table 7. In Figures 3−4 are shown the computed relative energies and properties as well as the fit functions for ϕ_{NO_2}, ($\tau^{min} = -42.64°$, ϕ_{NH_2}), and (τ, $\phi_{NH_2}{}^{min} = 2.77°$), where the superscript "min" denotes the value of the minimum structure. Figure 2 shows the fit functions $P(\tau, \phi_{NH_2})$.

The properties depend quite differently on the LAMs. The average dipole polarizability $\alpha_{av}^{(11)}$ changes little with (τ, ϕ_{NH_2})

TABLE 7: Fit Coefficients a_n, b_{ni} ($n = 0, 1, 2, 3$; $i = 0, 1, 2$) for the Relative Energies $\Delta E(\phi_{NO_2})$ and $\Delta E(\tau,\phi_{NO_2})$ According to Eqs 4 and 5

a_n	11.04957, −13.44937, 2.51922, −0.16654
b_{0i}	23.55194, −0.00871, 1.76554×10^{-6}
b_{1i}	−19.69167, 0.003501, -2.0325×10^{-7}
b_{2i}	1.29437, -4.587×10^{-3}, 4.01543×10^{-8}
b_{3i}	−0.09447, 2.67669×10^{-5}, -1.0704×10^{-9}

as well as with ϕ_{NO_2} (not shown), while the changes for μ and especially for the hyperpolarizabilities are much larger. The first hyperpolarizability $\beta_{||}$ is the most strongly affected property, which is probably due to the fact that the disruption of the conjugation path has a stronger effect on the first dipole-allowed excited state than on the ground state, due to its much larger charge separation. It is known that the difference of dipole moments of pNA in this state and in the ground state is to a large extent responsible for the large β_{xxx} value of pNA.[90] As for the amino inversion mode, all properties are seen to increase toward the planar configuration, as expected. We note that the computed relative energies for the two torsions are smaller than those computed at the DFT level by Chen and Chen.[6] The main reason for this difference is that the computations of Chen and Chen were performed on unrelaxed structures with a rotated amino or nitro group, while in our case, the rotated structures were relaxed with respect to all other degrees of freedom.

Additionally, it was checked whether the *frequency dispersion* also displays a strong mode dependence by performing frequency-dependent calculations at the RPA/D95V(p,d) level with λ = 1064 nm employing three nonminimum structures with 1, ϕ_{NO_2} = 30.8°; 2, (τ, ϕ_{NH_2}) = (37.36°, 22.77°); and 3, (τ, ϕ_{NH_2}) = (−42.64°, − 17.23°). These were compared with the minimum structure 4, (ϕ_{NO_2}, τ, ϕ_{NH_2}) = (0.8°, − 42.64°, 2.77°). The angle dependence of the dispersion may be estimated by the ratio $\beta_{||}^{\phi_{NH2},\phi_{NH2}}(-2\omega; \omega, \omega)/\beta_{||}^{\phi_{NO2},\phi_{NH2}}(0; 0, 0)$, for which we obtain the values 1.339, 1.347, 1.340, and 1.366 for the structures 1, 2, 3, and 4, respectively. These values show that the dependence of the dispersion on the torsional angles is rather small and, considering the approximate nature of the averaging procedure adopted here, may be neglected.

To compute the thermal average of the electrical properties $\langle P\rangle_\Omega$ according to

$$\langle P\rangle_\Omega = \int_0^\pi d\phi_{NH_2} \int_{-\pi/2}^{\pi/2} d\tau \int_0^\pi d\phi_{NO_2} P(\phi_{NO_2}, \tau, \phi_{NH_2}) \exp[-E(\phi_{NO_2}, \tau, \phi_{NH_2})/kT] \quad (6)$$

it was checked whether the three-variable functions (i.e., $P(\phi_{NO_2}$, τ, $\phi_{NH_2})$) could be approximated by assuming that the angles ϕ_{NO_2} and (τ, ϕ_{NH_2}) can be varied independently of each other. In this case, the energies are additive

$$E(\phi_{NO_2}, \tau, \phi_{NH_2}) = E(\phi_{NO_2}, \tau^{min}, \phi_{NH_2}^{min}) + E(\phi_{NO_2}^{min}, \tau, \phi_{NH_2}) \quad (7)$$

while the properties can be described by

$$P(\phi_{NO_2}, \tau, \phi_{NH_2}) = P(\phi_{NO_2}, \tau^{min}, \phi_{NH_2}^{min}) P(\phi_{NO_2}^{min}, \tau, \phi_{NH_2})/P(\phi_{NO_2}^{min}, \tau^{min}, \phi_{NH_2}^{min}) \quad (8)$$

This was done by simultaneously fixing all three dihedral angles at values away from the minimum structure, optimizing the remaining coordinates, and comparing the E and P for these partially optimized structures with those computed according to eqs 7 and 8. Three sets of values were used, (ϕ_{NO_2}, τ, ϕ_{NH_2})

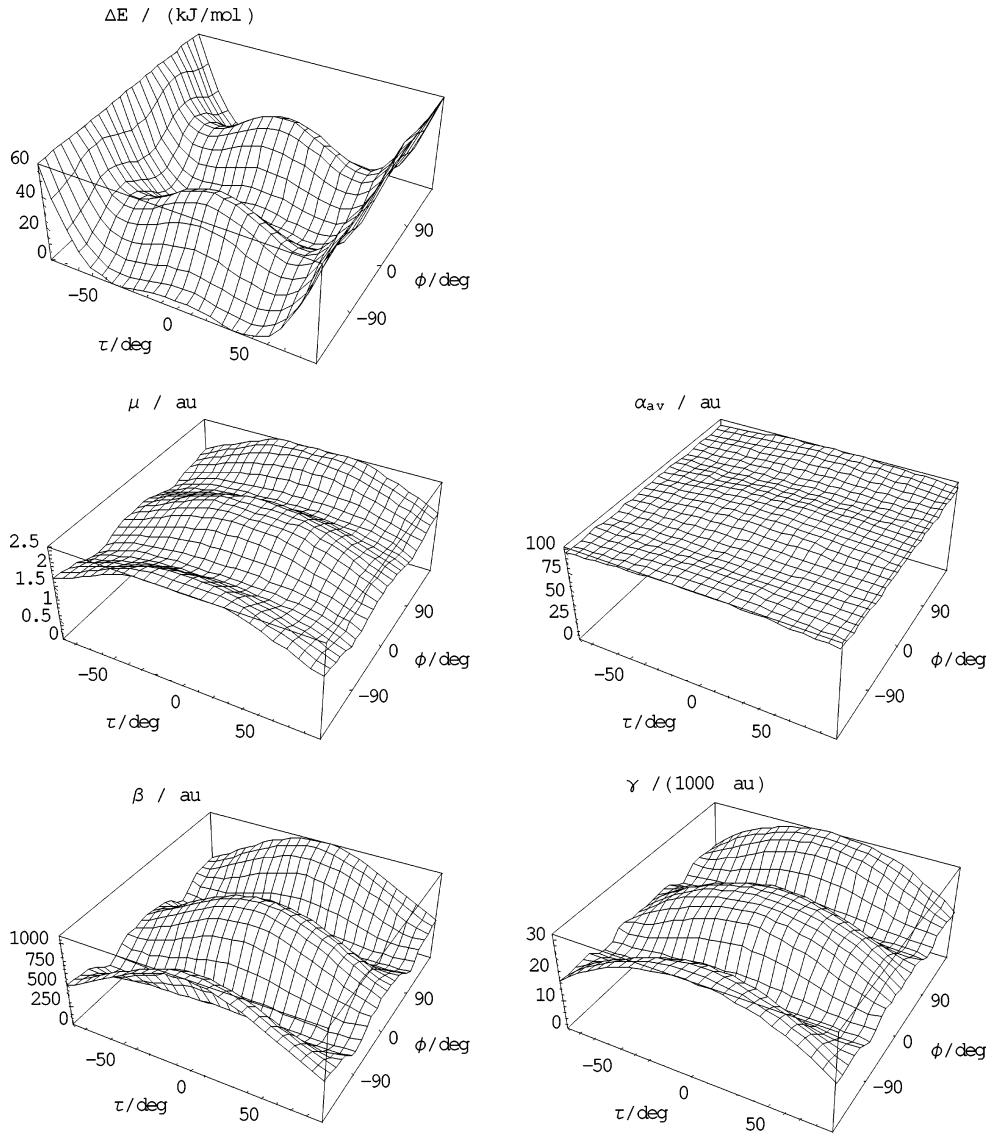

Figure 2. Fit functions of $P(\tau, \phi_{NH_2})$ ($P = \Delta E = E(\tau, \phi_{NH_2}) - E(\tau^{min}, \phi_{NH_2}^{min})$, μ, $\alpha_{av}^{(11)}$, $\beta_{||}$, γ_{av}) of pNA in the gas phase.

TABLE 8: Properties of pNA with Dihedral Angles (ϕ_{NO_2}, τ, ϕ_{NO_2}) = (17.46°, 22.77°, 20.8^0), (17.46°, 42.77°, 40.8°), (37.46°, −17.23°, 30.8°)[a]

	ΔE	μ	α_{av}	$\beta_{\|\|}$	γ_{av}
	(ϕ_{NO_2}, τ, ϕ_{NH_2}) = (17.46°, 22.77°, 20.8°)				
FF	9.955	2.493	100.59	926	29804
approx	9.633	2.574	100.61	926	29902
Δ	3.2%	−3.3%	0.0%	0.0%	−0.3%
	(ϕ_{NO_2}, τ, ϕ_{NH_2}) = (17.46°, 42.77°, 40.8°)				
FF	25.48	2.251	97.78	607	24353
approx	25.36	2.225	97.63	625	24718
Δ	0.5%	1.1%	0.2%	−2.7%	−1.5%
	(ϕ_{NO_2}, τ, ϕ_{NH_2}) = (37.46°, − 17.23°, 30.8°)				
FF	5.57	2.383	99.39	796	27107
approx	25.36	2.363	99.38	794	27089
Δ	6.9%	0.9%	0.0%	0.2%	0.1%

[a]Computed directly by the finite field (FF) method at the 6-31G**/MP2 (ΔE) or D95V(p,d)/MP2 (μ, α_{av}, $\beta_{||}$, γ_{av}) level and approximated with eqs 7 and 8 (approx). All units in au, except ΔE in kJ/mol.

= (17.46°, 22.77°, 20.8°), (17.46°, 42.77°, 40.8°), and (37.46°, − 17.23°, 30.8°), and the results in Table 8 show that the approximation is indeed reasonable, with relative differences for the energies smaller than 10% and for the properties smaller than 5%.

TABLE 9: Selected Properties *P* of pNA at the MP2/D95V(p,d) Level Relevant for EFISH at T = 470.05 K without ($P(\Omega^{min})$) and with ($\langle P \rangle_\Omega$) Averaging over the Three Dihedral Angles, Employing Eq 6

P	μ	$\beta_{\|\|}$	$\gamma_{av}/10^3$	$\mu\beta_{\|\|}$
$P(\Omega^{min})$	2.376	915	28.9	2175
$\langle P \rangle_\Omega$	2.351	837	28.0	1987
Δ	1.1%	9.4%	3.0%	9.5%

Using eqs 7 and 8 together with the fit functions in eq 6, the average properties in Table 9 were obtained. Only the average terms, which are relevant for the EFISH signal, are shown. T was set to 470.05 K as used in the experiment by Kaatz et al.[15] The effect on the μ, $\alpha_{av}^{(11)}$, and γ_{av} is small, but $\beta_{||}$ and $\mu\beta_{||}$, which gives the main contribution to the EFISH signal, decrease by about 10%.

Comparison with Experiment. Although there is an old gas-phase measurement of the dipole moment of pNA,[91] and the dipole moment obtained (2.20 ± 0.24 au) is in agreement with our value for the gas-phase geometry (2.39 au), the molecular beam method applied in that work is considered to be very difficult to interpret for large molecules such as pNA;[92] consequently, the reported values are probably not very reliable. More reliable are permittivity measurements in solution. Wortmann et al.[90] evaluated such measurements of pNA in 1,4-

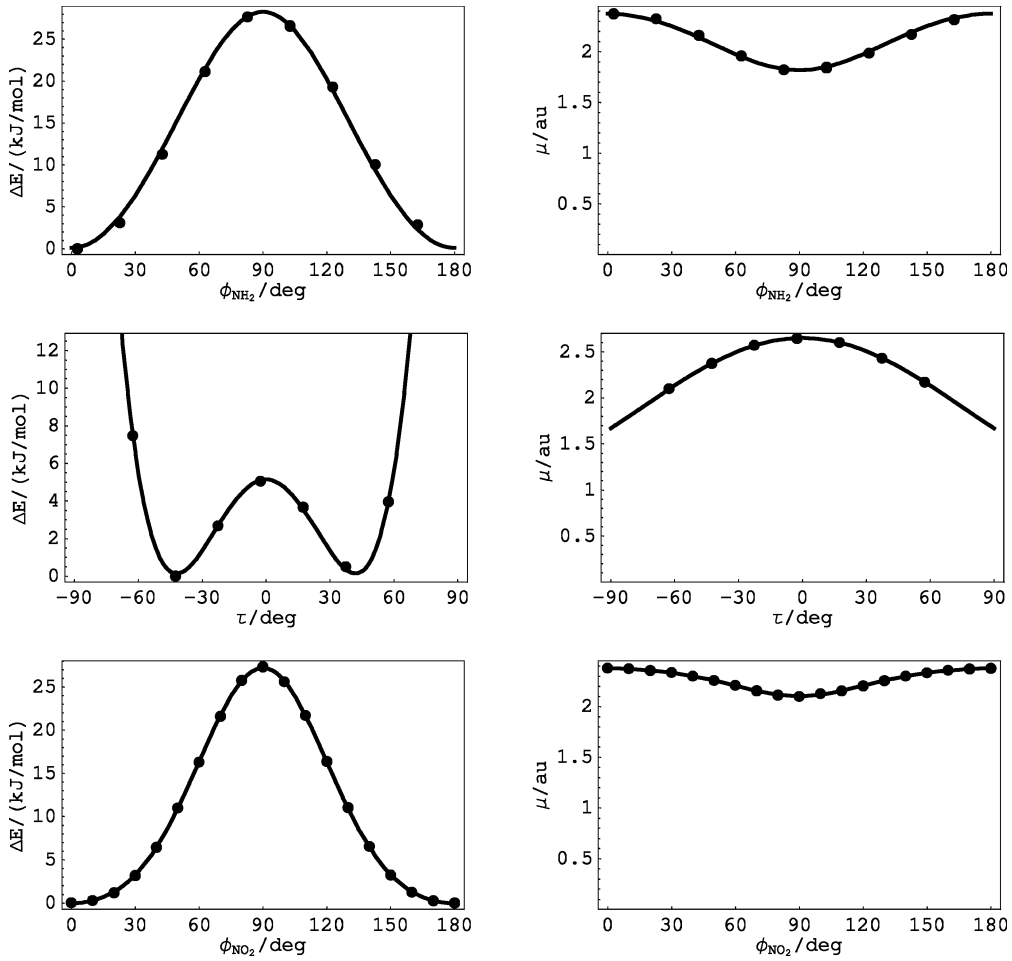

Figure 3. Computed values and fit functions of $\Delta E(\Omega)$ and $\mu(\Omega)$, ($\Omega = \phi_{NO_2}$, (τ, $\phi_{NH_2}^{min}$), (τ^{min}, ϕ_{NH_2})) of pNA in the gas phase.

dioxane solution, applying the ellipsoidal Onsager model to subtract the influence of the (linear) reaction field, and obtained $\mu = 2.45$ au. A similar value was obtained from electrooptical absorption measurements.[90] Cheng et al.[93] obtained 2.44 au in acetone solution, applying the spherical Onsager model. Stähelin et al.[94] employed a simplified form of the Guggenheim−Debye equation, which ignores the difference between internal and directing field and assumes a polar solute in a nonpolar solvent,[95] and combined it with spherical Onsager local field factors to estimate the dipole moment in 13 different, mostly polar solvents. Averaged over the solvents, their value is $\mu = 2.71 \pm 0.24$ au. These experimental values are 3−15% smaller than the comparable value of the 6-311G**/OSCRF/B3LYP structure at the MP2/Pol level obtained here, with the more accurate experimental values deviating more strongly. On the basis of a full π-valence MCSCF calculation, Mikkelsen et al.[3] suggested that a large static correlation effect may be responsible for the overestimation of μ computed with single reference determinant-based methods. However, we find that the more highly correlated multireference MRMP2 method yields nearly the same dipole moment as the correlated single-reference methods (see Table 3); therefore, this explanation appears to be ruled out.

To test if the discrepancy may be due to the LAMs, we performed a thermal average of the dipolar properties over the amino inversion mode in the same way as described in the previous section for the gas-phase structure, but applying the B3LYP/OSCRF/6-311G** model in the partial optimization computations. The fit of the relative energy ΔE (in kJ/mol) yields $\Delta E(\tau) = 0.1887 - 0.0418\psi^2 + 15.5282\psi$,[4] where ψ is the dihedral angle H−N−C−C (in rad). The relative change of the properties with respect to the minimum structure, computed at the MP2/D95V(p,d) level, is $\Delta\mu = 5.7\%$, $\Delta\alpha_{av}^{(11)} = 1.1\%$, $\Delta\beta_{||} = 9.0\%$, and $\Delta\gamma_{av} = 4.7\%$. Assuming that the amino and nitro torsions affect the dipole moment of the solution structure similarly as those of the gas-phase structure, the consideration of these modes would decrease μ by an additional 2−3%, leading then to an approximate computational value for μ of 2.5 au, which compares quite favorably with the experimental estimates.

Clearly, it cannot be ruled out that the dipolar Onsager model applied to extract the experimental dipole moment may be inadequate. Thus, only a direct experimental determination of the dipole moment of pNA in the *gas phase* can finally gauge the accuracy of the computed value.

A second value with which we can compare the computed values is the experimental EFISH measurement on pNA vapor at $T = 470.05$ K performed by Kaatz et al.[15] They report the average value $\langle\gamma\rangle_E = \mu\beta_{||}/(5kT) + \gamma_{av}$ as the primary result of the measurement. To extract $\beta_{||}$ from this quantity, they used the dipole moment computed by Sim et al.[12] for the *planar* geometry, which may be too large. We will thus use the experimental $\langle\gamma\rangle_E$ for comparison with our values. We computed two values for $\langle\gamma\rangle_E$, using different computational results. For the first value, the MP2/Pol values, scaled with the RPA dispersion, were used, for which all the components are available and no further approximations are necessary. For the second value, we took into account the CC2 dispersion and the thermal averaging over the considered LAMs This required further

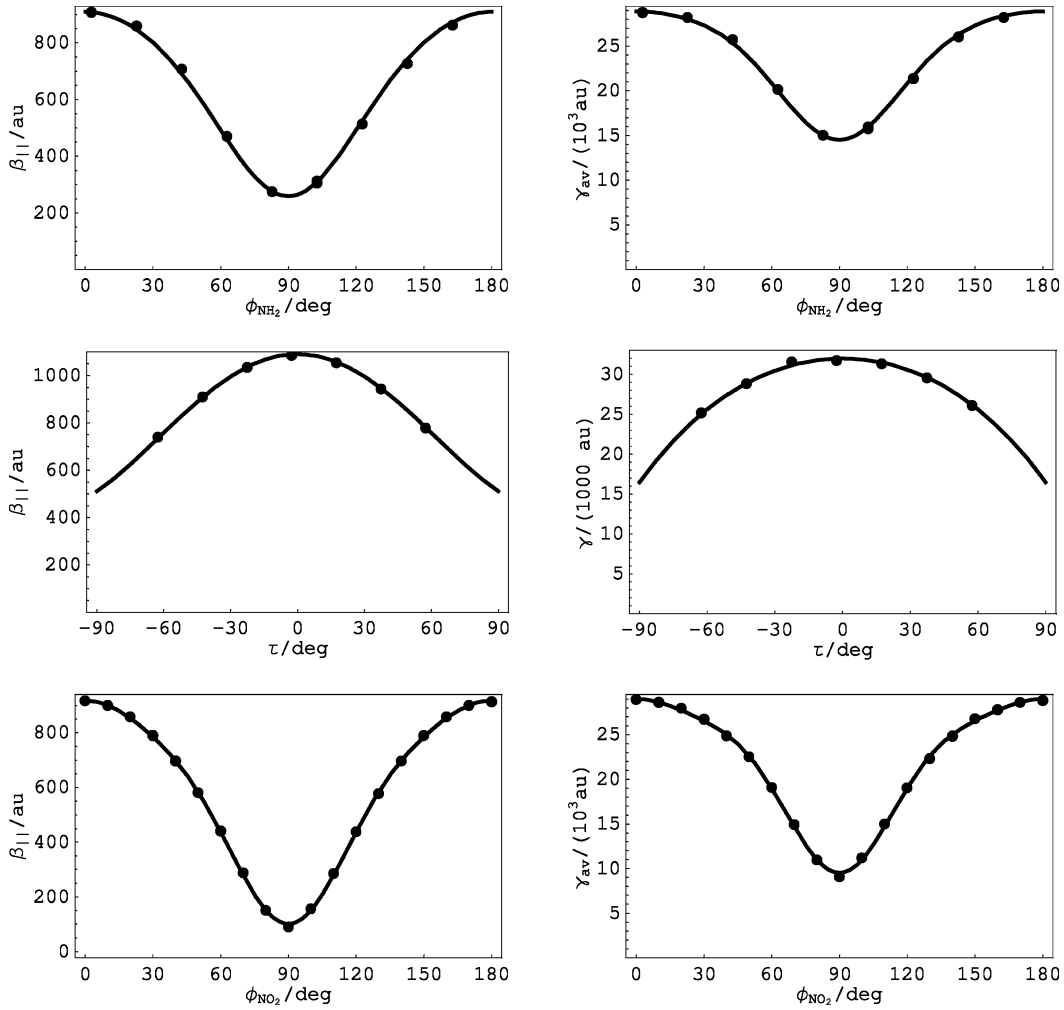

Figure 4. Computed values and fit functions of $\beta_{||}(\Omega)$ and $\gamma_{av}(\Omega)$, ($\Omega = \phi_{NO_2}$, (τ, $\phi_{NH_2}^{min}$), (τ^{min}, ϕ_{NH_2})) of pNA in the gas phase.

approximations. For the mode averaging, the properties at MP2/Pol level were scaled with the diminutions due to the LAMs computed at the MP2/D95V(p,d) level (see Table 8). To account for the CC2 dispersion, we considered that the dispersion of $\beta_{||}(-2\omega; \omega, \omega)$ is only slightly smaller than that of $\beta_{xxx}(-2\omega; \omega, \omega)$ both at the RPA level and at the CCSD level[22] and assumed that this is also valid for the CC2 level. Thus, the final value was computed from

$$\langle \mu\beta_{||}(-2\omega; \omega, \omega)\rangle_{\Omega} \approx \langle \mu\beta_{||}(0; 0, 0)\rangle_{\Omega} S_{xxx}(\mathrm{CC2}) \frac{S_{||}(\mathrm{RPA})}{S_{xxx}(\mathrm{RPA})} \quad (9)$$

where the S_k(Meth.) are scaling factors given by S_k(Meth.) = $\beta_k(-2\omega; \omega, \omega)$(Meth.)/$\beta_k(0; 0, 0)$(Meth.). A similar procedure was used to compute the contribution $\langle \gamma_{av}(-2\omega; \omega, \omega, 0)\rangle_{\Omega}$.

Computed and experimental values are shown in the last row of Table 4 [Note that contrary to ref 14 we assume that Kaatz et al.[15] defined the hyperpolarizabilities according to the Taylor series convention. This is in agreement with their definition of the susceptibility $\chi^{(3)}$(eq 1, 2 in ref 15); see also ref 21]. Both computed values are in reasonable agreement with the experimental value, with the RPA scaled value 1.4% and the probably more accurate CC2 scaled and mode-averaged value 5.6% larger than the experimental value. We note that the contribution of γ_{av} is 7% in the RPA scaled value and 10% in the CC2 scaled value.

As discussed above, the frequency dispersion of β may still be underestimated at the CC2/D95V(p,d) level and the value of γ_{av} at the MP2/Pol level may be underestimated due to missing static correlation effects. Both effects would therefore probably increase the CC scaled $\langle\gamma\rangle_E$ value again. On the other hand, the effects of a more accurate quantum mechanical treatment of the vibrational average, inclusion of field effects on the vibrational wave function, and consideration of vibrational effects on the frequency dispersion are difficult to estimate, but will probably not lead to changes larger than 10%.

Using the RPA scaled MP2/Pol properties computed for the C_{2v} structure leads to $\langle\gamma\rangle_E = 1.017 \times 10^3$ au, more than 40% larger than the experimental value. This may be taken as a further indication that the gas-phase geometry is indeed of C_s symmetry.

Electric Properties of Cyclohexane, Dioxane, and Tetrahydrofuran. The geometries of the three solvent molecules, CH, DI, and THF were optimized with the 6-311G** basis set using density functional theory (DFT), employing the B3LYP functional. See Figure 1 for the employed coordinate systems and symmetry groups for the optimized structures.

Table 10 shows selected components of the dipolar (hyper)-polarizabilities, multipole moments, and multipolar polarizabilities computed at the RHF level with the Pol, d-aug-cc-pVDZ, and aug-cc-pVTZ basis sets. All three basis sets yield very similar values for all properties; the largest deviations are found for γ_{av} but are within 5−8%, still quite small. This shows that the Pol basis set is adequate for these properties, probably also at the correlated level.

TABLE 10: Selected Static Dipolar Electrical Properties of CH, DI, and THF Calculated with the Pol, d-aug-cc-pVTZ (dDZ), and aug-cc-pVTZ (aTZ) Basis Sets at the RHF Level[a]

	CH			DI			THF		
BS	Pol	dDZ	aTZ	Pol	dDZ	aTZ	Pol	dDZ	aTZ
μ_x							0.7744	0.7735	0.7719
Q_{xx}	−15.2	−15.2	−15.1	−16.3	−16.3	−16.3	−13.2	−13.2	−13.1
Q_{zz}	−14.9	−14.9	−14.8	−13.5	−13.5	−13.4	−11.7	−11.6	−11.5
H_{xxxx}	−40.8	−40.3	−40.1	−31.5	−31.5	−31.3	−24.1	−24.1	−24.0
H_{zzzz}	−11.5	−11.0	−10.9	−9.5	−9.4	−9.2	−7.6	−7.4	−7.3
$\alpha_{av}^{(11)}$	67.73	66.87	66.80	52.51	52.72	52.65	48.78	48.94	48.89
$\beta_{\|\|}$							−32.4	−31.1	−31.1
γ_{av}	8983	8725	8375	6390	6627	6376	6082	6005	5783
$\alpha_{1,11}^{(12)}$							19.5	19.6	19.5
$\alpha_{3,13}^{(12)}$							9.9	10.0	10.0
$\alpha_{11,11}^{(22)}$	364	357	364	169	170	170	165	166	166
$\alpha_{22,22}^{(22)}$	364	357	364	280	282	283	207	208	207
$\alpha_{33,33}^{(22)}$	151	147	147	130	128	128	93	91	90
$\alpha_{12,12}^{(22)}$	198	198		146	147	147	115	116	116

[a] All units are in au (see ref 99 for conversion factors to other units).

TABLE 11: Static Electrical Properties of CH, DI, and THF, Calculated with the Pol Basis Set at the MP2 Level[a]

	CH	DI	THF
μ_x			0.7319
Q_{ii}	−15.4, −15.4, −15.2	−32.9, −23.6, −27.9	−13.3, −11.2, −11.9
Q_{xz}, Q_{yz}	0, 0	0.7, 0	0, −0.0
O_{iix}			0.45, −0.75, −0.28
O_{xyz}			0.24
H_{iiii};H_{xxyz}	−41.8, −41.8, −12.2; 0	−32.6, −32.9, −10.4; 0	−25, −25.8, −8.2; 0.4
H_{ijij};H_{yyyz}	−13.9, −9.2, −9.2; 0	−9.4, −7.0, −7.6; 0	7.9, −5.4, −5.5; 0.9
H_{xiiz};H_{zzzy}	−0.4, 0.4, 0; 0	−2.6, −1.1, −2.2; 0	0, 0, 0; 1.0
$\alpha_{ii}^{(11)}$	74.42, 74.42, 64.58	54.18, 63.51, 52.20	51.73, 56.98, 46.88
$\alpha_{av}^{(11)}$	71.14	56.63	51.86
$\alpha_{x,ii}^{(12)}$			19.4, −3.7, 1.6
$\alpha_{i,xz}^{(12)}$			0, 0.7, 9.8
$\alpha_{i,xy}^{(12)}$, $\alpha_{x,yz}^{(12)}$			0, 3.7, −0.2; 0.7
$\alpha_{ii,ii}^{(22)}$388, 388, 164		182, 293, 145	182, 224, 102
$\alpha_{ii,jj}^{(22)}$−33, −17, −17		0, −18, −7	−8, −3, 6
$\alpha_{ij,ij}^{(22)}$212, 133, 134		152, 68, 114	123, 75, 100
$\alpha_{xz,ii}^{(22)}$, $\alpha_{xy,yz}^{(22)}$	5, −5, 0; −5	6, −2, 23; 14	
$\alpha_{yz,ii}^{(22)}$, $\alpha_{xy,xz}^{(22)}$			−3, −2, −6; −8
β_{xii}			−43.5, −14.9, −11.5
$\beta_{\|\|}$			−42.0
γ_{iiii}	15171, 15171, 13988	8081, 12292, 14769	9681, 11333, 8301
γ_{iijj}	5040, 3674, 3674	3883, 3290, 4287	3376, 2421, 3877
γ_{av}	13820	11612	9733

[a] The index *i* runs over *x*, *y*, *z* and the double index *ij* runs over *xy*, *xz*, *yz*. All units are au (see ref 99 for conversion factors to other units).

Table 11 shows all the static electronic properties computed at the MP2 level with the Pol basis set for the three solvent molecules. Comparison with the RHF values of Table 10 shows that correlation has a considerable effect on γ, which is about 1.5 times larger at the MP2 level for all three molecules, while the other properties appearing in both tables are not greatly affected. The properties of CH are generally a bit larger than those of the other two molecules, while those of DI and THF are of comparable magnitude, except for those properties which are zero for 1,4-dioxane, due to its centrosymmetry.

To investigate the dependence of conformation on the dipolar properties, static (hyper)polarizabilities were computed for the two other conformers of 1,4-dioxane, which are local minima on the potential surface according to the computations of Chapman and Hester,[97] namely, the 1,4-twistboat (14TB) and the 2,5-twistboat (25TB) conformers. The geometries of the two conformers were first optimized at the DFT/B3LYP level with the 6-311G** basis. The average properties at the RHF/Pol level found for the 14TB conformer (symmetry D_2) were $\alpha_{av}^{(11)} = 52.13$ au (−2%), $\gamma_{av} = 5720$ au (−22%), and for 25TB (symmetry C_2), $\mu = 0.7$ au, $\alpha_{av}^{(11)} = 52.40$ au (−2%), $\beta_{\|\|} = -98$ au, $\gamma_{av} = 6355$ au (−10%), where the numbers in brackets indicate the differences to the chair conformer. Except for the properties which are nonzero in the noncentrosymmetric conformer 25TB and the γ values of 14TB, the conformation dependence is rather small. One should note, too, that the two conformers are much higher in energy than the chair conformer (30−40 kJ/mol acording to ref 97).

The static vibrational contributions, PV and ZPVA, to $\alpha^{(11)}$ and ZPVA contributions to γ of CH, DI, and THF are shown in Table 12. According to the procedure explained in section 2.1, all PV contributions shown in Table 12 can be considered converged at the DH approximation, except for $\alpha_{zz}^{(11)}$ of THF, where the more complete PV value is nearly eight times larger than the one at the DH level, which is already suspiciously large,

TABLE 12: Static PV, ZPVA, and Total Contributions to the Dipole−Dipole Polarizability $\alpha_{ii}^{(11)}$ and ZPVA Contributions to γ_{iijj} of CH, DI, and THF[a]

	CH		DI		THF	
	PV/RHF	ZPVA	PV/RHF	ZPVA	PV/RHF	ZPVA
$\alpha_{xx}^{(11)}$	0.69 (0.82)	3.19	5.70 (5.90)	1.80	1.90 (2.48)	18.6
$\alpha_{yy}^{(11)}$	0.69 (0.82)	3.19	6.94 (7.43)	2.58	3.87 (4.28)	2.22
$\alpha_{zz}^{(11)}$	1.06 (1.24)	2.68	8.02 (8.38)	1.93	27.33 (193)	2.00
α_{av}	0.81 (0.96)	3.02	6.89 (7.24)	2.10	11 (67)	2.03
	PV/MP2	total[b]	PV/MP2	total[b]	PV/MP2	total[c]
$\alpha_{xx}^{(11)}$	0.54	78.15	4.69	60.67	1.63	53.59
$\alpha_{yy}^{(11)}$	0.54	78.15	5.65	71.74	3.25	59.20
$\alpha_{zz}^{(11)}$	0.79	68.05	6.43	60.56	260	48.88
α_{av}	0.62	74.78	5.59	64.32	88	53.89
	ZPVA		ZPVA		ZPVA	
$\gamma_{xxxx},\gamma_{yyyy}$	414	414	98	336	100	214
$\gamma_{zzzz},\gamma_{xxyy}$	266	133	128	98	194	75
$\gamma_{xxzz},\gamma_{yyzz}$	74	74	42	67	74	97
γ_{av}		331		195		200

[a] PV contributions computed at the double harmonic (DH) level. Numbers in brackets show PV contributions including higher-order expansion terms; see text. All contributions computed at the RHF/6-311G** level, PV(DH) also at the MP2/6-311G** level. [b] $\alpha^{total}(0) = \alpha^{(11)elec.,\ MP2}(0) + \alpha^{(11)ZPVA,RHF}(0) + \alpha^{(11)PV,DH(MP2)}(0)$. [c] $\alpha^{total}(0) = \alpha^{(11)elec.,\ MP2}(0) + \alpha^{(11)ZPVA}(0)$.

especially at the MP2 level. Therefore, we will not consider any PV contributions to $\alpha_{ii}^{(11)}$ of THF in the computation of local fields in the liquids; the ZPVA contributions, however, look reasonable and should be taken into account. Apart from $\alpha_{zz}^{(11)}$ of THF, PV(DH) contributions at the MP2 and RHF levels are quite similar. The total values, which will be used in the computations of the permittivities, are also shown in Table 12.

Frequency-dependent values of CH and DI at the RPA and at the multiplicatively scaled MP2 level, as well as total values obtained by adding the scaled ZPVA values to the scaled MP2 values, are shown in Table 13. The frequency dependence of $\alpha(-\omega; \omega)$, $\alpha(-3\omega; 3\omega)$, and $\gamma(-3\omega; \omega, \omega, \omega)$ at $\lambda = 2\pi c/\omega = 1907$ nm is small, well below 10%. This gives confidence that the error introduced by the rather low level used for the computation of the dispersion (RPA) will not lead to large deviations for the macroscopic susceptibilities computed with the RPA scaled property values. We are not aware of any experimental gas-phase results with which we could compare our computed values.

4. Conclusions

In this study, we computed multipole moments up to hexadecapole, polarizabilities up to quadrupole−quadrupole, and dipole hyperpolarizabiltites of cyclohexane, 1,4-dioxane, tetrahydrofuran, and *p*-nitroaniline, including vibrational contributions and frequency dispersion for the dipolar properties. For CH, DI, and THF, different basis sets were compared and showed the adequacy of the selected Pol basis set. Due to its larger size, no thorough basis set study could be performed for pNA; however, comparison of the performance of Pol with the smaller basis set D95V(p,d) and with results in the literature using the aug-cc-pVDZ basis set as well as a stripped-down version of the aug-cc-pVTZ basis set suggest that for the dipole properties up to β both Pol and D95V(p,d) yield values close to the basis set limit, while for γ and the higher-order polarizabilities, Pol may be superior to D95V(p,d).

An investigation of the convergence behavior of the pure vibrational contributions to the dipolar properties of pNA and of $\underline{\underline{\alpha}}^{(11)}$ of the three solvent molecules has been performed. We concluded that only the PV contributions to $\underline{\underline{\alpha}}^{(11)}$ of CH and DI are converged at the lowest level of perturbation theory and possibly also the PV contributions of $\underline{\boldsymbol{\beta}}$ of pNA on the next higher order. However, these conclusions have to be considered with caution, as not all derivative terms for a complete evaluation of the highest perturbational order were available. We note that, of all the computed PV contributions here, those of $\underline{\underline{\alpha}}^{(11)}$ are the most relevant for the computation of the macroscopic susceptibilities of EFISH and hyper-Rayleigh scattering (HRS) experiments, as they influence both the permanent and the induced local field directly. The influences of $\underline{\boldsymbol{\beta}}$ and $\underline{\underline{\boldsymbol{\gamma}}}$ on the local fields are usually very small, and the influence of the PV to $\underline{\boldsymbol{\beta}}$ on the EFISH and HRS signals should be small, as only fields at optical frequencies are involved.

For pNA, the geometry optimization in the gas phase as well as in nonpolar solvents using self-consistent reaction field methods leads to a pyramidalized amino group, if polarized basis sets are employed. In polar solvents, the OSCRF optimization yields a nearly planar amino group. The effects of these geometry changes on the largest contribution to the EFISH signal, $\mu\beta_{\parallel}$, is not negligible, and an analysis in terms of structural parameters shows that the amino group pyramidalization has the largest effect, while the shortening of the two C−N bonds in the solvated structure yield nearly all the

TABLE 13: Frequency-Dependent Electronic and Total Dipole−Dipole Polarizabilities $\alpha^{(11)}(-\omega; \omega)$ and Second Hyperpolarizabilities for THG $\gamma(-3\omega; \omega, \omega, \omega)$ at $\lambda = 2\pi/(hc\omega) = 1907$ nm of CH, DI, and THF Computed at the RPA/Pol//6-311G/B3LYP and (scaled MP2)/Pol//6-311G**/B3LYP Levels[a]**

	CH			DI			THF		
	RPA	Sc. MP2	total[b]	RPA	Sc. MP2	total[b]	RPA	Sc. MP2	total[b]
$\alpha_{xx}^{(11)}$	70.84	74.55	77.75	50.62	54.91	56.73	48.34	51.82	53.68
$\alpha_{yy}^{(11)}$	70.84	74.55	77.75	60.46	64.49	67.11	53.64	57.08	59.30
$\alpha_{zz}^{(11)}$	61.86	64.70	67.39	48.84	53.06	55.02	44.62	46.96	49.04
$\alpha_{av}^{(11)}$	67.85	71.27	74.30	53.31	57.49	59.62	48.87	51.95	54.01
γ_{1111}	10268	16075	16514	4897	8483	8586	5917	10244	10351
γ_{2222}	10268	16075	16514	7554	13074	13431	7173	11993	12219
γ_{3333}	10154	14962	15247	8706	15944	16082	6077	8787	8989
γ_{1122}	3423	5340	5481	2380	4115	4219	2270	3572	3652
γ_{1133}	2526	3875	3953	2050	3488	3533	1669	2562	2640
γ_{2233}	2526	3875	3953	2459	4578	4650	2482	4103	4205
γ_{av}	9532	14664	15015	6996	12388	12596	6407	10299	10511

[a] Deviations from Kleinmann symmetry are smaller than 1%. [b] $P^{Total}(\omega) = P^{elec.,ScaledMP2}(\omega) + P^{ZPVA,\ ScaledRPA}(\omega)$.

remaining contribution to the changes. These findings may be compared with those of Cammi et al.,[98] who found similar solvent-induced effects on (hyper)polarizabilities of donor−acceptor substituted polyenes using the polarizable continuum model in the integral equation formalism (IEFPCM) in water as the solvent. In that work, the effects were interpreted in terms of the bond-length alternation (BLA) parameter, which indicated a change from polyene-like structures in the gas phase to partially ionic structures in the solvent. For pNA, however, the pyramidaliztion of the amino group seems to be at least equally important for the dipolar properties as the solvent-induced bond length changes. We showed that in the case of pNA the application of more sophisticated polarized continuum methods than the dipolar OSCRF leads to similar values for the dipolar electric properties, although the quantitative changes between the gas-phase and solvated structures were found to be smaller.

The effect of thermal averaging over the two substituent groups torsion modes on the dipolar properties of pNA was investigated, too, and was found to have a nonnegligible influence on the EFISH signal. Taking all the effects into account, the only experimental EFISH value reported in the literature could be reproduced. Using instead the properties computed for the structure obtained for the geometry in polar solvents leads to pronounced disagreement with the experimental datum. For the molecular dipole moment of pNA, which has been reliably measured only in the liquid phase, discrepancies remain which may be due to the neglect of other large-amplitude motions neglected here or to the Onsager model applied to obtain the experimental dipole moment.

Clearly, the effects of large-amplitude motions and solvent-induced geometry effects on (hyper)polarizabilities may be even more relevant for other donor−acceptor molecules, which are, overall, larger and/or have larger mobile groups, like N-substituted pNA derivatives, p,p′-substituted stilbenes, tolanes, and so on. Several computational examples of such effects have been published already in the literature, for example, in refs 26 and 27.

We stress finally that all the properties computed here are still those of the *single* molecule. The effect of the solvent environment on these properties in quadrupolar approximation and the (non)linear optical susceptibilities of the pure liquids cyclohexane, 1,4-dioxane, and tetrahydrofuran as well as solutions of pNA in these solvents will be investigated in the framework of the discrete local field theory in the second part of this series.

Acknowledgment. We gratefully acknowledge financial support from the European Commission in the form of a Marie Curie Development Host Fellowship (HPMD-CT-2001-00091).

References and Notes

(1) Rice, J. E.; Shelton, D. P. *Chem. Rev.* **1994**, *94*, 3.
(2) Cammi, R.; Mennucci, B.; Tomasi, J. *J. Phys. Chem. A* **1998**, *102*, 870.
(3) Mikkelsen, K. V.; Luo, Y.; Ågren, H.; Jørgensen, P. *J. Chem. Phys.* **1994**, *100*, 8240.
(4) Jensen, L.; van Duijnen, P. Th.; Snijders, J. G. *J. Chem. Phys.* **2003**, *119*, 3800.
(5) Jensen, L.; Swart, M.; van Duijnen, P. Th. *J. Chem. Phys.* **2005**, *122*, 034103.
(6) Gubskaya, A. V.; Kusalik, P. G. *J. Chem. Phys.* **2002**, *117*, 5290.
(7) Janssen, R. H. C.; Bomont, J.-M.; Theodorou, D. N.; Raptis, S.; Papadopoulos, M. G. *J. Chem. Phys.* **1999**, *110*, 6463.
(8) Reis, H.; Papadopoulos, M. G.; Theodorou, D. N. *J. Chem. Phys.* **2001**, *114*, 876.
(9) Poulsen, T. D.; Ogilby, P. R.; Mikkelsen, K. V. *J. Chem. Phys.* **2001**, *115*, 7843.
(10) Gubskaya, A. V.; Kusalik, P. G. *Mol. Phys.* **2001**, *99*, 1107.
(11) Clays, C. *J. Nonlinear Opt. Phys. Mater.* **2003**, *12*, 475.
(12) Sim, F.; Chin, S.; Dupuis, M.; Rice, J. E. *J. Phys. Chem.* **1993**, *97*, 1158.
(13) Luo, Y.; Ågren, H.; Vahtras, O.; Jørgensen, P. *Chem. Phys. Lett.* **1993**, *207*, 190.
(14) Salek, P.; Vahtras, O.; Helgaker, T.; Ågren, H. *J. Chem. Phys.* **2002**, *117*, 9630.
(15) Kaatz, P.; Donley, E. A.; Shelton, D. P. *J. Chem. Phys.* **1997**, *108*, 849.
(16) Teng, C. C.; Garito, A. F. *Phys. Rev. B* **1983**, *28*, 6766.
(17) Ledger, M. B.; Suppan P. *Spectrochim. Acta* **1967**, *23A*, 3007.
(18) Baumann, W. in *Physical Methods of Chemistry*; Rossiter, B. W., Hamilton, J. F., Eds.; Wiley: New York, 1989; Vol. 3B, p 45.
(19) Khajehpour, M.; Kauffman, J. F. *J. Phys. Chem. A* **2001**, *105*, 10316.
(20) Geerlings, J. D.; Varma, C. A. G. O.; van Hemert, M. C. *J. Phys. Chem. B* **2000**, *104*, 56.
(21) Kaatz, P.; Shelton, D. P. *J. Chem. Phys.* **1996**, *105*, 3918.
(22) Salek, P.; Helgaker, T.; Vahtras, O.; Ågren, H.; Jonsson, D.; Gauss, J. *Mol. Phys.* **2005**, *103*, 439.
(23) Trueblood, K. N.; Goldish, E.; Donohue, J. *Acta Crystallogr.* **1961**, *14*, 1009.
(24) Colapietro, M.; Domenicano, A.; Marciante, C.; Portalone, G. *Z. Naturforsch.* **1982**, *37b*, 1309.
(25) Wang, C.-K.; Wang, Y.-H.; Su, Y.; Luo, Y. *J. Chem. Phys.* **2003**, *119*, 4409.
(26) Lipinski, J.; Bartkowiak, W. *Chem. Phys.* **1999**, *245*, 263.
(27) Bartkowiak, W.; Misiaszek, T. *Chem. Phys.* **2000**, *261*, 353.
(28) Farztdinov, V. M.; Schanz, R.; Kovalenko, S. A.; Ernsting, N. P. *J. Phys. Chem. A* **2000**, *104*, 11486.
(29) Velders, G. J. M.; Giller, J.-M.; Becker, P. J.; Feil, D. *J. Phys. Chem.* **1991**, *95*, 8601.
(30) Eckart, U.; Sadlej, A. J. *Mol. Phys.* **2001**, *99*, 735.
(31) Torrent-Sucarrat, M.; Solà, M.; Duran, M.; Luis, J. M. *J. Chem. Phys.* **2002**, *116*, 5363.
(32) Torrent-Sucarrat, M.; Solà, M.; Duran, M.; Luis, J. M. *J. Chem. Phys.* **2004**, *120*, 6346.
(33) Applequist, J. *Chem. Phys.* **1984**, *85*, 279; **1995**, *190*, 153 (erratum).
(34) Dykstra, C.; Liu, S.-L.; Malik, D. J. *Adv. Chem. Phys.* **1989**, *75*, 37.
(35) Logan, D. E. *Mol. Phys.* **1982**, *46*, 271.
(36) Gunning, M. J.; Raab, R. E. *Mol. Phys.* **1997**, *91*, 589.
(37) Ward, J. F.; New, G. H. C. *Phys. Rev.* **1969**, *185*, 57.
(38) Burland, D. M.; Walsh, C. A.; Kajzar, F.; Sentein, C. *J. Opt. Soc. Am. B* **1991**, *8*, 2269.
(39) Sadlej, A. J. *Col. Cz. Chem. Commun.* **1988**, *53*, 1995.
(40) Norman, P.; Luo, Y.; Ågren, H. *J. Chem. Phys.* **1997**, *107*, 9535.
(41) Reis, H.; Papadopoulos, M. G.; Munn, R. W. *J. Chem. Phys.***1998**, *109*, 6828.
(42) Pluta, T.; Noga, J.; Bartlett R. J. *Int. J. Quantum Chem.: Quantum Chem. Symp.* **1994**, *28*, 379.
(43) Woon, D. E.; Dunning, T. H. *J. Chem. Phys.* **1994**, *100*, 2975.
(44) Dunning, T. H. *J. Chem. Phys.* **1989**, *90*, 1007.
(45) Kendall, R. A.; Dunning, T. H.; Harrison, R. J. *J. Chem. Phys.* **1992**, *96*, 6796.
(46) Woon, D. E.; Dunning, T. H. *J. Chem. Phys.* **1994**, *98*, 1538.
(47) Woon, D. E.; Dunning, T. H. *J. Chem. Phys.* **1995**, *103*, 4572.
(48) Basis sets were obtained from the Extensible Computational Chemistry Environment Basis Set Database, Version 2/12/03, as developed and distributed by the Molecular Science Computing Facility, Environmental and Molecular Sciences Laboratory, which is part of the Pacific Northwest Laboratory, P.O. Box 999, Richland, WA 99352, U.S.A., and funded by the U.S. Department of Energy. The Pacific Northwest Laboratory is a multiprogram laboratory operated by Battelle Memorial Institue for the U.S. Department of Energy under contract DE-AC06-76RLO 1830. Contact David Feller or Karen Schuchardt for further information.
(49) Jensen, H. J. Aa.; Ågren, H. *Chem. Phys. Lett.* **1984**, *110*, 140.
(50) Olsen, J.; Jørgensen, P. *J. Chem. Phys.***1985**, *82*, 3235.
(51) Nakano, H. *J. Chem. Phys.* **1993**, *99*, 7983.
(52) Nakano, H. *Chem. Phys. Lett.* **1993**, *207*, 372.
(53) Ågren, H.; Vahtras, O.; Koch, H.; Jørgensen, P.; Helgaker, T. *J. Chem. Phys.* **1993**, *98*, 6417.
(54) Christiansen, O.; Koch, H.; Jørgensen, P. *Chem. Phys. Lett.* **1995**, *244*, 75.
(55) Cohen, H. D.; Roothaan, C. C. J. *J. Chem. Phys.* **1965**, *43*, S34.
(56) Jensen, F. *Introduction to Computational Chemistry*; Wiley: Chichester, 1999.
(57) Frisch, M. J.; Trucks, G. W.; Schlegel, H. B.; Scuseria, G. E.; Robb, M. A.; Cheeseman, J. R.; Zakrzewski, V. G.; Montgomery, J. A., Jr.; Stratmann, R. E.; Burant, J. C.; Dapprich, S.; Millam, J. M.; Daniels, A. D.; Kudin, K. N.; Strain, M. C.; Farkas, O.; Tomasi, J.; Barone, V.; Cossi, M.; Cammi, R.; Mennucci, B.; Pomelli, C.; Adamo, C.; Clifford, S.; Ochterski, J.; Petersson, G. A.; Ayala, P. Y.; Cui, Q.; Morokuma, K.; Malick,

D. K.; Rabuck, A. D.; Raghavachari, K.; Foresman, J. B.; Cioslowski, J.; Ortiz, J. V.; Stefanov, B. B.; Liu, G.; Liashenko, A.; Piskorz, P.; Komaromi, I.; Gomperts, R.; Martin, R. L.; Fox, D. J.; Keith, T.; Al-Laham, M. A.; Peng, C. Y.; Nanayakkara, A.; Gonzalez, C.; Challacombe, M.; Gill, P. M. W.; Johnson, B. G.; Chen, W.; Wong, M. W.; Andres, J. L.; Head-Gordon, M.; Replogle, E. S.; Pople, J. A. *Gaussian 98*, revision A.9; Gaussian, Inc.: Pittsburgh, PA, 1998.

(58) Helgaker, T.; Jensen, H. J. Aa. Joergensen, P.; Olsen, J.; Ruud, K.; Aagren, H.; Auer, A. A.; Bak, K. L.; Bakken, V.; Christiansen, O.; Coriani, S.; Dahle, P.; Dalskov, E. K.; Enevoldsen, T.; Fernandez, B.; Haettig, C.; Hald, K.; Halkier, A.; Heiberg, H.; Hettema, H.; Jonsson, D.; Kirpekar, S.; Kobayashi, R.; Koch, H.; Mikkelsen, K. V.; Norman, P.; Packer, M. J.; Pedersen, T. B.; Ruden, T. A.; Sanchez, A.; Saue, T.; Sauer, S. P. A.; Schimmelpfennig, B.; Sylvester-Hvid, K. O.; Taylor, P. R.; Vahtras O. Dalton, a molecular electronic structure program; release 1.2; 2001, http://www.kjemi.uio.no/software/dalton/dalton.html.

(59) Schmidt, M. W.; Baldridge, K. K.; Boatz, J. A.; Elbert S. T.; Gordon, M. S.; Jensen, J. H.; Koseki, S.; Matsunaga, N.; Nguyen, K. A.; Su, S. J.; Windus, T. L.; Dupuis, M.; Montgomery, J. A. *J. Comput. Chem.* **1993**, *14*, 1347.

(60) Bishop, D. M. *Adv. Chem. Phys.* **1998**, *104*, 1.

(61) Reis, H.; Papadopoulos, M. G.; Avramopoulos, A. *J. Chem. Phys. A* **2003**, *107*, 3907.

(62) Rauk, A.; Allen, L. C.; Clementi, E. *J. Chem. Phys.* **1970**, *52*, 4133.

(63) Bock, C. W.; George, P.; Trachtman, M. *Theor. Chim. Acta* **1986**, *69*, 235.

(64) Bludský, O.; Šponer, J.; Leszcynski, J.; Špirko, V.; Hobza, P. *J. Chem. Phys.* **1996**, *105*, 11042.

(65) Chen, P. C.; Chen, S. C. *Comput. Chem.* **2002**, *26*, 171; Rashid, A. N.; *J. Mol. Struct. (Theochem)* **2004**, *681*, 57.

(66) Schlegel, H. B.; McDouall, J. J. W. In *Computational Advances in Organic Chemistry: Molecular Structure and Reactivity*; Ögretir, C., Csizmadia, I. G., Eds.; Kluwer: Dordrecht, 1991; p167.

(67) Cancés, E.; Mennucci, B.; Tomasi, J. *J. Chem. Phys.* **1997**, *107*, 3032.

(68) Barone, V.; Cossi, M. *J. Phys. Chem. A* **1998**, *102*, 1995.

(69) Champagne, B. *Chem. Phys. Lett.* **1996**, *261*, 57.

(70) Cammi, R.; Frediani, L.; Mennucci, B.; Ruud, K. *J. Chem. Phys.* **2003**, *119*, 5818.

(71) Alparone, A.; Millefiori, A.; Millefiori, S. *Chem. Phys. Lett.* **2005**, *312*, 261.

(72) Harrand, M. *J. Raman Spectrosc.* **1975**, *4*, 53.

(73) Kozich, V.; Werncke, W.; Dreyer, J.; Brzezinka, K.-W.; Rini, M.; Kummrow, A.; Elsaesser, T. *J. Chem. Phys.* **2002**, *117*, 719.

(74) Moran, A. M.; Kelley, A. M. *J. Chem. Phys.* **2001**, *115*, 912.

(75) Ågren, H.; Vahtras, O.; Koch, H.; Jørgensen, P.; Helgaker, T. *J. Chem. Phys.* **1993**, *98*, 6417.

(76) Hättig, C.; Jørgensen, P. *J. Chem. Phys.* **1998**, *109*, 2762.

(77) Millefiori, S.; Favinii, G.; Millefiori, A.; Grasso, D. *Spectrochim. Acta* **1977**, *33A*, 21.

(78) Bertinelli, F.; Palmieri, P.; Brillante, A.; Taliani, C. *Chem. Phys.* **1977**, *25*, 333.

(79) van Gisbergen, A. J. A.; Snijders, J. G.; Baerends, E. J. *J. Chem. Phys.* **1998**, *109*, 10644; **1999**, *111*, 6652 (erratum).

(80) Scott, A. P.; Radom, L. *J. Phys. Chem.* **1996**, *100*, 16502.

(81) Champagne, B.; Perpète, E. A.; van Gisbergen, S. J. A.; Baerends, E.-J.; Snijders, E.-J.; Soubra-Gaoui, C.; Robins, K. A.; Kirtman, B. *J. Chem. Phys.* **1998**, *109*, 10489; **1999**, *110*, 11664 (erratum).

(82) van Gisbergen, S. J. A.; Schipper, P. R. T.; Gritsenko, O. V.; Baerends, E. J.; Snijders, J. G.; Champagne, B.; Kirtman, B. *Phys. Rev. Lett.* **1999**, *83*, 694.

(83) Champagne, B.; Perpète, E. A.; Jacquemin, D.; van Gisbergen, S. J. A.; Baerends, E.-J.; Soubra-Gaoui, C.; Robins, K. A.; Kirtman, B. *J. Phys. Chem. A* **2000**, *104*, 4755.

(84) Gritsenko, O. V.; van Gisbergen, S. J. A.; Schipper, P. R. T.; Baerends, E. J. *Phys. Rev. A* **2000**, *62*, 012507.

(85) Gritsenko, O. V.; Baerends, E. J. *Phys. Rev. A* **2001**, *64*, 042506.

(86) Bishop, D. M.; Luis, J. M.; Kirtman, B. *J. Chem. Phys.* **1998**, *108*, 10013.

(87) Luis, J. M.; Duran, M.; Champagne, B.; Kirtman, B. *J. Chem. Phys.* **2000**, *113*, 5203.

(88) Torrent-Sucarrat, M.; Luis, J. M.; Kirtman, B. *J. Chem. Phys.* **2005**, *122*, 204108.

(89) Yamada, S.; Yamaguchi, K.; Kamada, K.; Ohta, K. *Mol. Phys.* **2003**, *101*, 309.

(90) Wortmann, R.; Krämer, P.; Glania, C.; Lebus, S.; Detzer N. *Chem. Phys.* **1993**, *173*, 99.

(91) Estermann, I.; Wohlwill, M. *Z. Phys. Chem.* **1933**, *B20*, 195.

(92) Dugourd, P.; Compagnon, I.; Lepine, F.; Antoine, R.; Rayane, D.; Broyer, M. *Chem. Phys. Lett.* **2001**, *336*, 511.

(93) Cheng, L.-T.; Tam, W.; Stevenson, S. H.; Meredith, G. R.; Rikken, G.; Marder, S. R. *J. Phys. Chem.* **1991**, *95*, 10631.

(94) Stähelin, M.; Burland, D. M.; Rice, J. E. *Chem. Phys. Lett.* **1992**, *191*, 245.

(95) Boettcher, C. J. F.; Bordewijk, P. *Theory of electric polarization*; Elsevier: Amsterdam, 1978; Vol. II.

(96) Foresman, J. B.; Keith, T. A.; Wiberg, K. B.; Snoonian, J.; Frisch, M. J. *J. Phys. Chem.* **1996**, *100*, 16098.

(97) Chapman, D. M.; Hester, R. E. *J. Chem. Phys.* **1997**, *A101*, 3382.

(98) Cammi, R.; Mennucci, B.; Tomasi, J. *J. Am. Chem. Soc.* **1998**, *120*, 8834.

(99) Conversion factors from au to other unit systems. μ: 1 au = 2.5417 $\times$ 10^{-18} esu = 8.4784 $\times$ 10^{-30} C m. *Q*: 1 au = 1.3450 $\times$ 10^{-26} esu = 4.4866 $\times$ 10^{-40} C m^2. *O*: 1 au = 7.1176 $\times$ 10^{-35} esu = 2.3742 $\times$ 10^{-50} C m^3. *H*: 1 au = 3.7665 $\times$ 10^{-43} esu = 1.2564 $\times$ 10^{-60} C m^4. $\alpha^{(11)}$: 1 au = 1.4818 $\times$ 10^{-25} C m^3 = 0.16488 $\times$ 10^{-40} C^2 m^2 J^{-1}. $\alpha^{(12)}$: 1 au = 7.8413 $\times$ 10^{-34} C m^4 = 8.7251 $\times$ 10^{-52} C^2 m^3 J^{-1}. $\alpha^{(22)}$: 1 au = 4.1494 $\times$ 10^{-42} C m^5 = 4.6171 $\times$ 10^{-62} C^2 m^4 J^{-1}. β: 1 au = 0.86394 $\times$ 10^{-30} esu = 3.2066 $\times$ 10^{-53} C^3 m^3 J^{-2}. γ: 1 au = 5.0372 $\times$ 10^{-40} esu = 6.2360 $\times$ 10^{-65} C^4 m^4 J^{-3}.